Construction and Building Materials 461 (2025) 139920

Contents lists available at ScienceDirect

Construction and Building Materials

journal homepage: www.elsevier.com/locate/conbuildmat

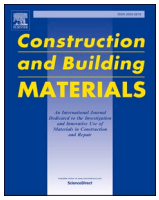

Mechanism and effect of Re-curing on strength recovery of fire-damaged high strength engineered cementitious composite

S. Rawat [a,b], C.K. Lee [b], D.J. Fanna [c], L. George [c], Y.X. Zhang [a,*]

[a] Centre for Advanced Manufacturing Technology, School of Engineering, Design and Built Environment, Western Sydney University, NSW 2751, Australia
[b] School of Engineering and Technology, The University of New South Wales, Canberra, ACT 2600, Australia
[c] Advanced Materials Characterisation Facility, Western Sydney University, NSW, 2116, Australia

ARTICLE INFO

Keywords:
Elevated temperature
Engineered cementitious composite
Post-fire curing
Rehydration
Residual compressive strength

ABSTRACT

This study presents novel investigation into the restoration of fire-damaged high strength engineered cementitious composites (HSECC) through re-curing, focusing on how factors like re-curing duration and binder material selection influence the strength recovery process. Five types of HSECC mixes constituting blends of ground granulated blast furnace slag (GGBFS), fly ash, dolomite, silica fume, hybrid polyethylene and steel fibres were first exposed to temperatures ranging from 200°C-800°C, followed by three different types of re-curing including air curing for 28 days or water curing for 7–28 days. A comprehensive testing program was implemented, including detailed compressive stress-strain tests and microstructural analyses using techniques such as SEM, XRD, TG/DSC, and MIP to assess the effects of mix composition and curing methods. Test results showed that post-fire curing in air did not lead to any appreciable strength recovery with no clear evidence of rehydration after 28 days. On the contrary, curing in water resulted in substantial strength recovery, particularly in specimens exposed to 400–600°C, where recovered strength even exceeded the room temperature strength. Microstructural analysis confirmed that water curing promotes the formation of rehydration products, such as ettringite and portlandite, which effectively fill microcracks and voids caused by fibre melting, resulting in a refined pore-size distribution. Although all mixes showed significant recovery after water re-curing, the extent recovery was influenced by the severity of initial thermal damage. These effects were also found to be closely related to the binder type, with GGBFS-based mixes demonstrating superior performance. The study further proposes a possible mechanism for the re-curing process based on these findings.

1. Introduction

Fire is severely detrimental to reinforced concrete structures due to the drastic degradation and damage it may cause at various stages depending on the exposure degree, time, and area. The conventional rehabilitation of the fire-damaged concrete structures usually requires removal of the damaged concrete and replacement with the fresh pitching material, epoxy or mortar grouting, and bonding with fibre reinforced polymer sheets or through other similar techniques which are time and resource intensive. In response to these challenges, researchers are constantly trying to analyse the efficacy of autogenous methods such as self-healing method to reduce this cost. Post-fire curing has emerged as one of the most novel approaches to partially recover the mechanical properties and durability performance of fire-damaged concrete without any repair. Existing literatures have also demonstrated promising outcomes with the application of this measure.

Poon et al. [1] studied the effect of post-fire curing on the strength of normal and high strength concrete and observed better recovery in blended concrete as compared to plain concrete. Mixes with different ratio of fly ash (FA), silica fume, ground granulated blast furnace slag (GGBFS) and metakaolin were considered and FA-based concrete showed the maximum recovery due to the rehydration reaction between portlandite and unhydrated FA particles. On the other hand, Akca and Ozyurt [2] observed better compressive strength recovery in concrete containing GGBFS compared to that with pulverized FA. Vyšvařil et al. [3] compared the rehydration in blended cement paste mixed with ground limestone, GGBFS, and FA. They found that while GGBFS was effective in maintaining high strength at elevated temperatures, it did not contribute significantly to recovery during re-curing. Ground limestone, however, was more beneficial for promoting rehydration. Recent

* Corresponding author.
E-mail address: sarah.zhang@westernsydney.edu.au (Y.X. Zhang).

https://doi.org/10.1016/j.conbuildmat.2025.139920
Received 2 November 2024; Received in revised form 22 December 2024; Accepted 6 January 2025
Available online 9 January 2025

Table 1
Mix parameters for this study.

Mix ID	Binder (proportions in %)					Fibre (% vol.)		Room temperature properties	
	Cement	GGBFS	FA	Dolomite	Silica fume	PE	Steel	Compressive strength (MPa)	Elastic modulus (GPa)
M1	40	37.5	7.5	15	-	1.50	0.75	138.1	36.5
M2	45	37.5	7.5	10	-	1.50	0.75	142.4	38.2
M3	40	37.5	7.5	15	-	1.25	1	145.2	38.6
M4	50	50	-	-	-	1.50	0.75	143.7	35.9
M5	90	-	-	-	10	1.50	0.75	153.7	38.3

studies by Wang et al. [4] and Li et al. [5] focused on ultra-high-performance concrete with and without silica fume. Their findings indicated that the healing process was more pronounced in mortars without silica fume. This was due to the formation of ettringite in the silica fume-containing mixes, which filled the pores and caused expansive forces, potentially diminishing the healing effect. Moreover, the inclusion of carbon black nanoparticles and multi-walled carbon nanotubes has been found to enhance strength recovery by providing additional nucleation sites during re-curing [6,7]. Additionally, carbonation curing, and water-CO_2 cyclic curing have also demonstrated significant improvements in strength recovery [5,8].

In general, while post-fire water curing has shown to improve the strength of fire-damaged concrete, the extent of recovery with different supplementary cementitious materials (SCMs) is not well understood. Li et al. [9] conducted a comprehensive review on post-fire curing effects but could not establish a clear trend in recovery with various pozzolanic materials due to limited research in this area. This is particularly important for engineered cementitious composites (ECC), which typically contain higher amounts of SCMs than conventional concrete. SCMs such as FA, silica fume, limestone calcined clay blends, rice husk ash, GGBFS, and waste glass powder [10–15] are commonly used in ECC to promote pozzolanic reactions. However, their use may lower the calcium-silica ratio, which is not conducive to rehydration due to their low reactivity [5]. Additionally, structures containing ECC are more vulnerable to fire due to the low permeability and dense microstructure, and it remains unclear whether rehydration would be beneficial or detrimental to its performance. On one hand, the vacant channels created by low melting point fibres in ECC may facilitate moisture infiltration, enhancing rehydration. On the other hand, rehydration might cause the formation of calcium hydroxide or ettringite, leading to volume expansion and further deterioration of the matrix [9]. Therefore, findings from conventional concrete cannot be generalized to ECC, highlighting the need for further research in this area to broaden the understanding of post-fire curing effects on this material to promote its engineering application.

The present study attempts to bridge this gap by comprehensively investigating the influence of post-fire curing on the compressive performance of high strength ECC (HSECC) and subsequently understanding the nature of recovery mechanism. To the authors' knowledge, no prior studies have examined the combined effects of SCMs and fibre content on post-fire curing while considering various re-curing methods. Previous research by the authors indicated that a quaternary blend of GGBFS, dolomite powder, and FA demonstrated superior performance at room temperature and exhibited excellent strength retention (45–47 % at 800°C) at elevated temperatures [16–19]. Building on these findings, this study analyses recovery of the previously used binder systems under three re-curing methods, i.e. 7 days of water curing, 28 days of water curing, and 28 days of air curing. The extent of recovery is analysed through the measurement of compressive stress-strain behavior after thermal exposure and re-curing. Scanning electron microscopy (SEM), X-ray diffraction (XRD), thermogravimetric analysis (TGA), differential scanning calorimetry (DSC) and mercury intrusion porosimeter (MIP) techniques are further employed to characterize the microstructure, phase development, and change in porosity after rehydration.

Table 2
Re-curing conditions adopted in the present study.

ID	Re-curing type	Re-curing condition	Testing day after air cooling
A28	28 days air	20°C and 55 % RH	28th day
W7	7 days water	20°C and 95 % RH	8th day (dried for one day after completion of curing regime)
W28	28 days water	20°C and 95 % RH	29th day (dried for one day after completion of curing regime)

2. Experimental programs

2.1. Raw materials and mixes

The binder materials included cement and SCMs namely GGBFS, FA, dolomite powder and silica fume. Fine sand passing through a 300-micron sieve was used as the main aggregate, with a constant sand-binder ratio of 0.36 for mixes M1-M4 and 0.40 for mix M5. The water-binder ratio was kept constant at 0.20 for all mixes. Additionally, poly-carboxylic ether-based high range water reducer (HRWR) was used to maintain the flowability of the mix. Hybrid fibre reinforced HSECC was designed using polyethylene (PE) fibre with a length of 12 mm and an aspect ratio of 500 and steel fibre with a length of 13 mm and an aspect ratio of 65. The specific mix parameters, along with the room-temperature compressive strength and elastic modulus, are detailed in Table 1. These mechanical properties were sourced from the authors' previous work [18] and are presented here for comparison.

The five mixes (M1-M5) were selected to examine the individual effects of the binder system and fibre content on recovery following thermal exposure. The main mixes (M1-M3) were designed to achieve a higher cement replacement ratio, with 60 % of the cement replaced by SCMs. These mixes demonstrated superior residual compressive and tensile strength after exposure to elevated temperatures and air cooling in authors' previous study [18]. For comparison, a standard mix (M5) containing silica fume and a mix (M4) with only GGBFS (cement: GGBFS ratio of 50:50) were utilized. Mix M3 differed from M1 primarily in fibre proportion; M3 contained 1.25 % PE and 1 % steel fibre, whereas M1 had 1.5 % PE and 0.75 % steel fibre. More details on the mix design selection, exact mix proportions, and mix development can be found in the authors' previous work [16,18].

2.2. Specimen preparation and heat treatment

Cylinders of size 75 mm diameter × 150 mm height were cast and cured at 23°C and 95 % relative humidity (RH) for 28 days and 20°C and 55 % RH for another 28 days following similar procedure as adopted in Rawat et al. [18]. Thereafter, the specimens were put in the furnace and exposed to 200, 400, 600, and 800°C at 1 °C/min with 2 hours dwelling period. After the completion of the heating, the specimens were allowed to naturally cool in air. They were then exposed to different re-curing conditions as highlighted in Table 2. A comprehensive investigation was conducted on the effect of re-curing using compressive stress-strain tests, and the results were further analysed through detailed

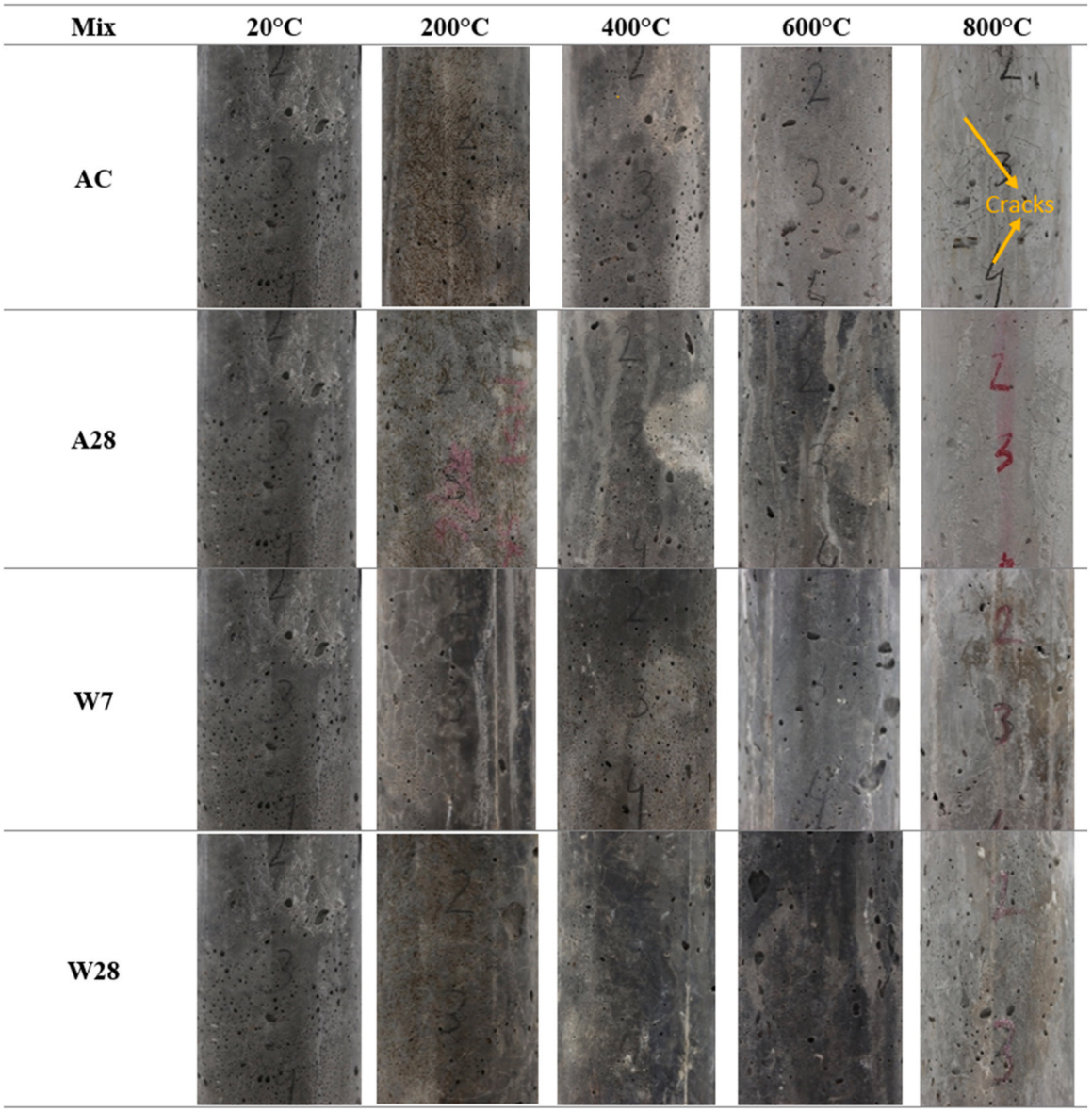

Fig. 1. Surface texture of M5 mix specimens after air cooling and re-curing.

microstructural analysis, as explained in the following section. The re-curing tests results were also compared with the air-cooled (AC) specimens tested immediately after cooling. The effect of air-cooling on the same binder composition has been systematically elaborated upon in the authors' previous work [18], and the same results have been utilized for comparison in the present study.

2.3. Testing programs

2.3.1. Uniaxial compression tests

A 3000 kN capacity compression testing machine was used to obtain the stress-strain curve and elastic modulus of the HSECC specimens after re-curing. Compression tests were conducted at a displacement rate of 0.05 mm/min, whereas load-controlled rate of 0.25 MPa/sec was used for estimation of elastic modulus. The specimen notation used is 'MX-T-Z,' where MX represents the mix ID (X = 1…5), T indicates the exposure temperature (ranging from 200 to 800°C), and Z denotes the cooling or re-curing method such that AC means air cooled specimens tested without any re-curing (detailed results presented in [18]), A28 means re-curing for 28 days in air, W7 means re-curing for 7 days in water and W28 means re-curing for 28 days in water. For example, M1–400-W7 refers to M1 mix specimens exposed to 400°C, followed by 7 days of water re-curing before compression testing. Three cylinders were tested per case, resulting in a total of 300 specimens (5 mix designs × 5 temperatures × 4 post-exposure stage × 3 specimens). It should be noted that the elastic modulus data for series M5–600-A28 was not reported due to experimental complications.

2.3.2. Characterisation methods

Characterisation methods were employed on the samples collected from each set of tested specimens for microstructural study. Initially, the solid samples were stored in small containers filled with acetone to remove moisture. The samples were then placed in a desiccator under vacuum for the first 48 hours, followed by drying at 60°C for an additional 24 hours.

A small portion of the solid sample was used for SEM analysis, employing a Phenom XL scanning electron microscope. Each sample was coated with carbon using Leica EM SCD005 sputter coater to make a conductive surface. Subsequently, the samples were analysed in the SEM under 15 kV and 1 Pa chamber pressure. MIP analysis was also

Fig. 2. A closer look on M5 specimens' surface after air cooling and water re-curing.

conducted on solid samples to determine the pore size distribution after air cooling and re-curing. A sample size of 3–5 mm was subjected to pressures ranging from 0.10 to 60,000 psi (0.7 kPa to 413.7 MPa) with a contact angle of 130°. The volume of mercury intruded was recorded at each pressure level to determine the pore size characteristics.

The remaining dried sample was ground into fine powder (<300 microns) for XRD and TG/DSC analysis. XRD analysis was done on samples prepared in back-loaded holders to minimize preferred orientation effects. The samples were analysed using a Bruker D8 Advance powder diffractometer equipped with a LynxEye XE-T position-sensitive detector. Diffraction patterns were collected in Bragg–Brentano geometry with Cu-Kα radiation, operating at 40 kV and 40 mA. The scan range covered 5–80° 2θ, with a step size of 0.02° and a counting time of 2.5 seconds per step. Phase identification was performed using Bruker Eva v6 software, in conjunction with the 2022 Powder Diffraction File (PDF4 +) database from the International Centre for Diffraction Data. Furthermore, TG/DSC analysis was performed on the same powdered sample using a Netzsch STA 449F5 Jupiter to analyse the thermal decomposition process and mass loss at varying temperatures. The mass of the sample was fixed to 50 ± 0.5 mg for each measurement. The tests were implemented following a heating procedure from 40°C to 1000°C under nitrogen flow and a heating rate of 10 °C/min.

3. Results and discussions

3.1. Effect of heating and re-curing on the physical characteristics

A quick assessment of the effect of re-curing can be made through the visual inspection of surface texture and colour change. Fig. 1 shows M5 mix specimens after thermal exposure and post-exposure re-curing. The surface texture and colour of the specimens which underwent 28 days re-curing in air closely resembled the air-cooled specimens. Across all HSECC mixes, the colour progressively changed from grey/black to light white as the exposure temperature increased from 200°C to 800°C. Air re-curing also helped reduce the severity of surface cracks, with visibly fewer cracks at 800°C in all mixes compared to air-cooled specimens.

However, the effect of re-curing in water was different than that of specimens re-cured in air. Re-curing in water led to significant improvement in the surface texture and this further improved with increase in the duration. As shown in Fig. 2, the cracks caused by thermal damage were no longer easily visible in the specimens re-cured in water for 28 days. The colour of the water re-cured specimens remained relatively similar till 600°C exposure and tended to become more closer to the control (ambient temperature) specimens.

3.2. Residual compressive strength

3.2.1. Effect of type of re-curing

The residual compressive strength of the HSECC specimens is significantly affected by exposure temperature [18]. However, post-exposure curing has been identified as an effective repair technique, leading to considerable enhancements in performance and this trend was consistent across all mixes. Fig. 3 shows the comparison of the effect of different post-curing types with non-cured specimens at different temperature range (with variation ranges of the three specimens). It is evident that the general trend for both air and water re-curing was similar across all specimens within the considered temperature range.

Post-exposure curing in air did not lead to any significant improvement in strength. The difference between the strength of air-cooled specimens and the 28-day air re-cured specimens was minimal, possibly due to experimental variations or surface rehydration depending on the matrix composition. All mixes retained relatively high residual strength at lower temperatures under air re-curing, but the strength showed little change compared with air-cooled specimens. For instance, at 400°C, M1 specimens retained 77 % of their strength, which increased slightly to 78 % after 28-day re-curing. Similarly, for M5 exposed to 400°C, the retention remained almost unchanged, from 77 % to 76 %, when comparing air-cooled specimens with 28-day air re-cured specimens. This trend was similar at higher temperatures and M5 exhibited lower strength due to higher thermal degradation and cracking, likely resulting from its denser microstructure.

However, post-exposure re-curing in water showed a significant improvement which was temperature dependent. Specimens exposed to 200°C and re-cured in water initially showed a decrease in strength. Previous studies have also reported similar decrease, which was attributed to water penetrating the capillary and gel pores, leading to a loose structure of C-S-H [20] or the depolymerization of silicate in C-S-H due to moisture absorption [21,22]. This likely caused a 13 % strength decrease at 7 days, but only a 3–11 % reduction at 28 days due to more pronounced rehydration.

Conversely, specimens exposed to higher temperatures demonstrated significant improvement. The improvement was particularly notable between 400°C and 600°C, with strength retention increasing with the duration of re-curing. For instance, M1 specimens showed an average retention of 79.8 % in strength after 7 days of water re-curing at 400°C, which increased to 83.1 % after 28 days of water re-curing. Overall, a strength increase of 1–18 % was observed in the 7-day re-cured specimens, further improving by approximately 5–10 % after 28 days of re-curing. The improvement in 600°C exposed specimens was more pronounced, with around a 40 % increase in residual compressive strength compared to the non-re-cured specimens after 28 days of curing. In some cases, the strength was even greater than the original room temperature compressive strength. This could be attributed to the denser microstructure formed during rehydration compared to the control specimens. As the fibres melt, the mix becomes more homogeneous, improving water penetration and enabling better hydration of available sites. Additionally, the absence of polymer fibres, which may have reduced strength in the control specimens, allowed the newly formed hydration products to fill these spaces, resulting in a denser matrix and, consequently, higher strength.

At 800°C, since specimens experienced significant degradation from thermal exposure, the resulting retention was lower compared to those exposed to 600°C. However, the strength recovery relative to air-cooled specimens remained substantial. The strength recovery at this temperature was around 5–26 % on 7-day water re-curing which further increased to 22–55 % on 28-day re-curing. The degree of this recovery was influenced by the extent of prior thermal damage, the availability of

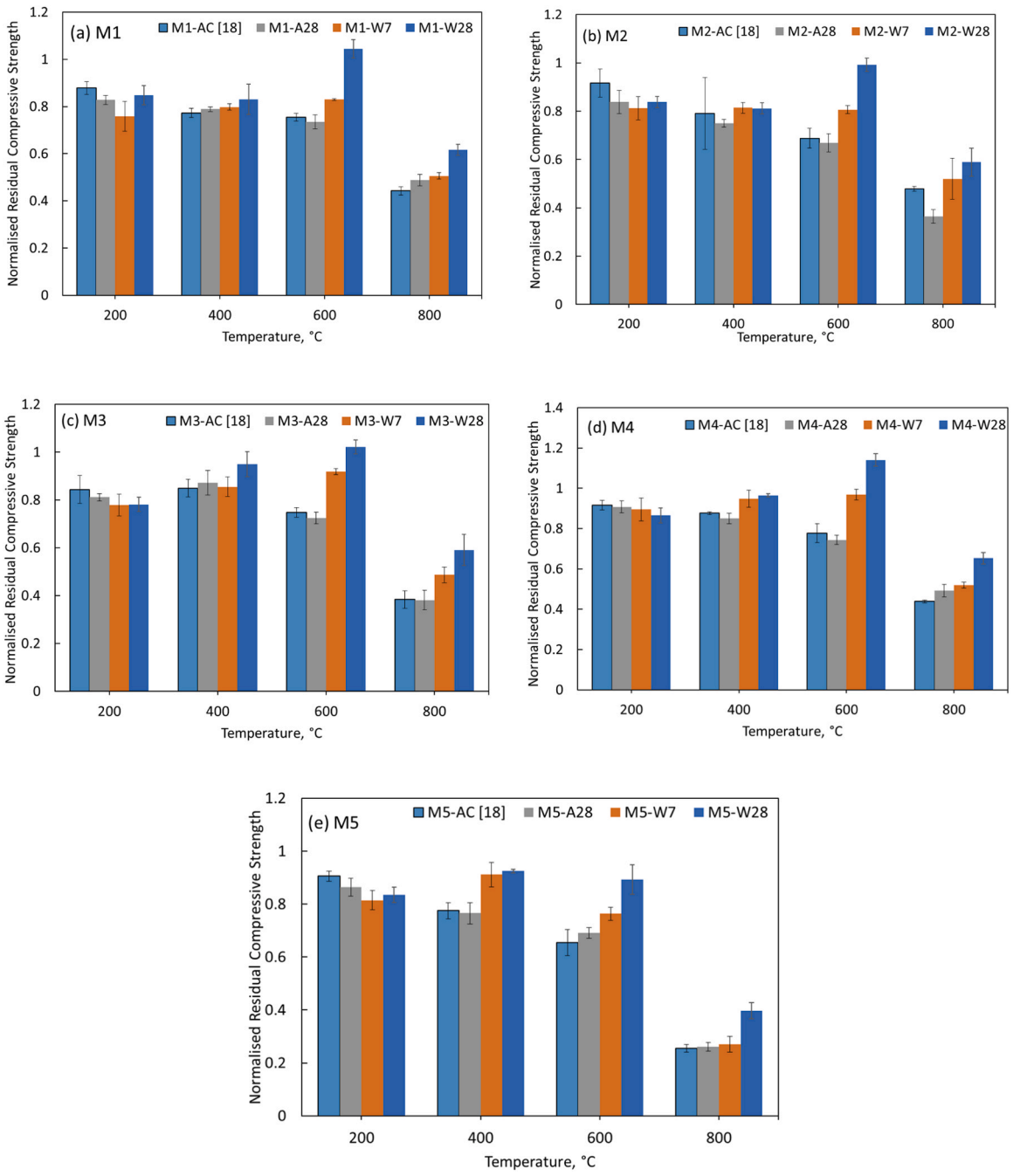

Fig. 3. Comparison of the residual compressive strength of HSECC mix specimens after different re-curing stages.

rehydration sites, and the porosity to accommodate any resulting expansion. Consequently, the type of SCM used also played a critical role in the rehydration process, as discussed in the following section.

3.2.2. *Effect of type of SCM*

Fig. 4 shows the normalised residual compressive strength of M1 to M5 cylinder specimens for different re-curing types. As previously noted, air re-curing had a similar effect to air cooling, with M5 showing the greatest strength reduction due to its dense microstructure and lack of improvement with air re-curing. M1 and M4 exhibited higher residual strength due to a thermally better performing matrix and optimized fibre proportions [18]. Mix M3 specimens (with higher steel fibre content but lower PE fibre content than M1) initially exhibited comparable strength but experienced a significant reduction at 800°C, with no improvement from air re-curing. The overall effect of fibres at elevated temperatures depends on a combination of factors: better pore pressure dissipation from melting of PE fibres or more effective crack control from the presence of steel fibres. At lower temperatures, where matrix decomposition is still controlled, steel fibres in M3 provided effective crack bridging, while PE fibres in M1 helped reduce cracking by better dissipating pore pressure. However, at higher temperatures, steel fibres in M3 became ineffective, and the reduced dissipation of pore pressure likely led to the poorer performance of M3 compared to M1.

On the other hand, water re-cured specimens showed significantly better performance. Water re-curing promotes rehydration, leading to the formation of secondary hydration products, such as C-S-H, portlandite, and ettringite, which can help fill voids in the matrix. For instance, at 600°C, M1 demonstrated 82 % strength retention after 7 days of water re-curing, compared to 75 % for air-cooled specimens. Similarly, at 800°C, M1 retained 50 % of its strength after 7 days of

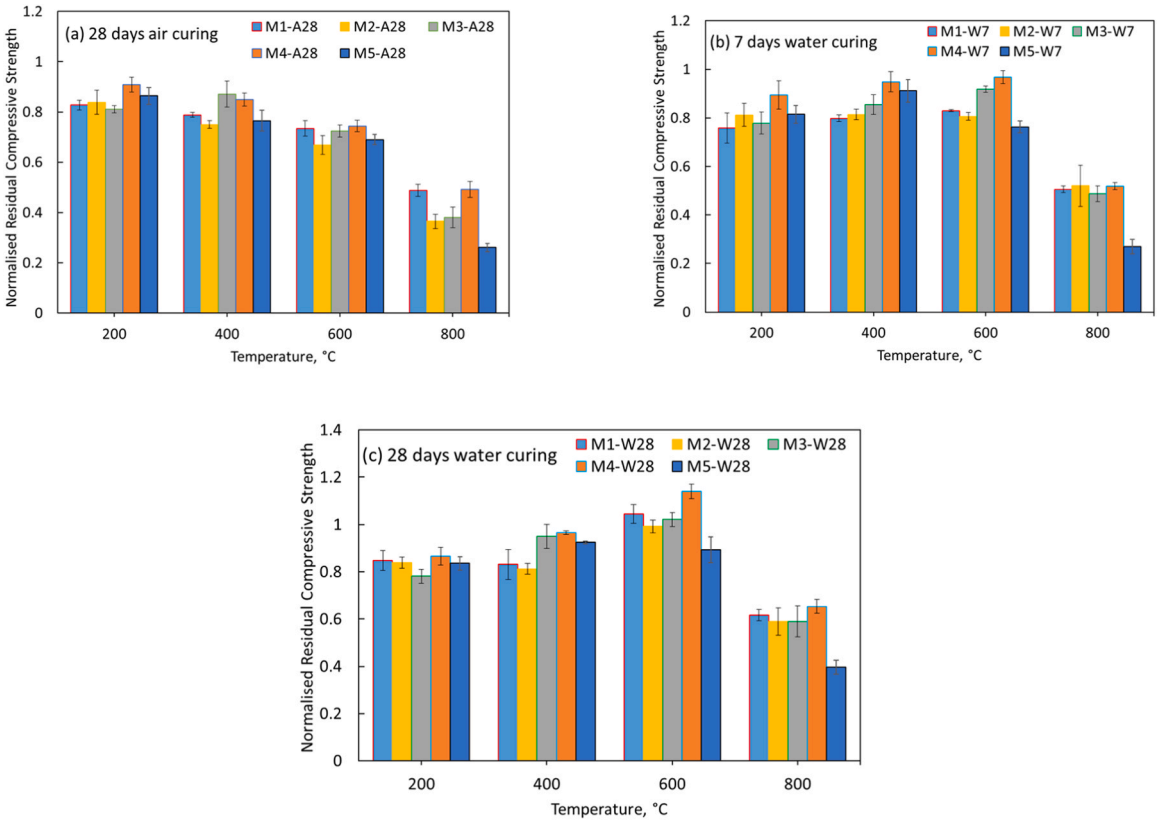

Fig. 4. Residual compressive strength of HSECC specimens after elevated temperature exposure and (a) 28 days re-curing in air (b) 7 days re-curing in water (c) 28 days re-curing in water.

water re-curing, compared to 44 % for air-cooled specimens, showing a recovery of 10 % and 14 %, respectively at 600°C and 800°C. After 28 days of water curing, this recovery increased to 38–39 % at 600–800°C, indicating significant strength improvement.

Mix M2, which had a higher cement content and lower dolomite content than M1, showed relatively lower recovery at 800°C, with around 22 % strength increase compared to air-cooled specimens. The higher recovery in M1 may be due to the better filling effect of dolomite, or its higher rehydration potential compared to decomposed cement. Mix M3, which had a similar matrix composition to M1 but a different fibre proportion, demonstrated even greater recovery than M1. After 7-day water re-curing, 800°C-exposed M3 specimens showed 26 % improvement, which increased to 54 % after 28 days of water re-curing. The strength after recovery followed a similar trend to the residual strength after thermal exposure, likely due to the mechanism described earlier. The role of steel fibres might have been more dominant until 600°C, as they provided better bonding with the rehydration products, improving crack bridging and strength recovery. Mix M4, a binary blend of GGBFS and cement, also showed improvements similar to M1 after 7-day re-curing (15.2 %) but exhibited a slightly higher improvement at 28 days of water re-curing (48 %). Similarly, Mix M5 showed a substantial increase in strength after 28-day water re-curing, with a 55 % increase compared to 39 % for M1 at 800°C.

This recovery may be attributed to the rehydration of CaO, which improves with extended curing time. The expansion resulting from the conversion of CaO into calcium hydroxide (CH) or the generation of ettringite may have been accommodated within the pores created by water evaporation and fibre melting. Furthermore, rehydration products like CH can dissolve in water, partially offsetting expansion and leading to better improvements after 28 days of water re-curing. The

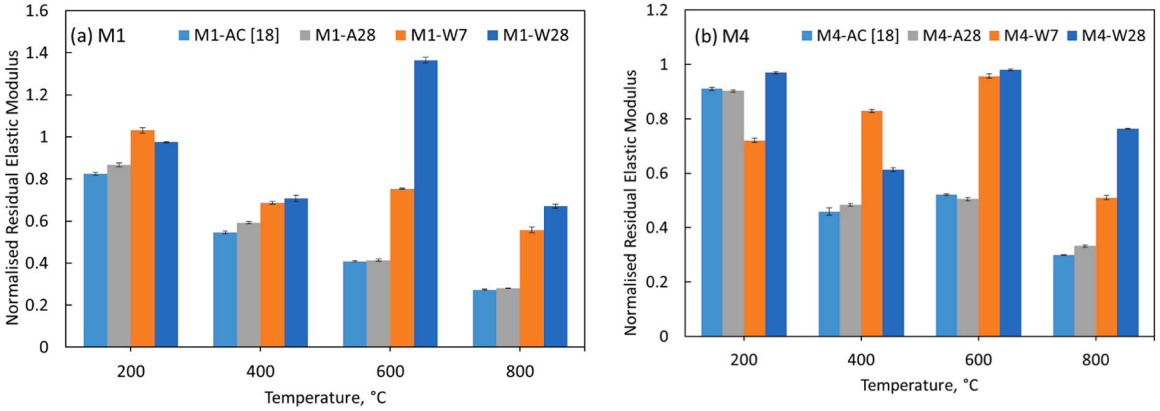

Fig. 5. Comparison of residual elastic modulus of air cooled and post-fire cured M1 and M4 mix specimens.

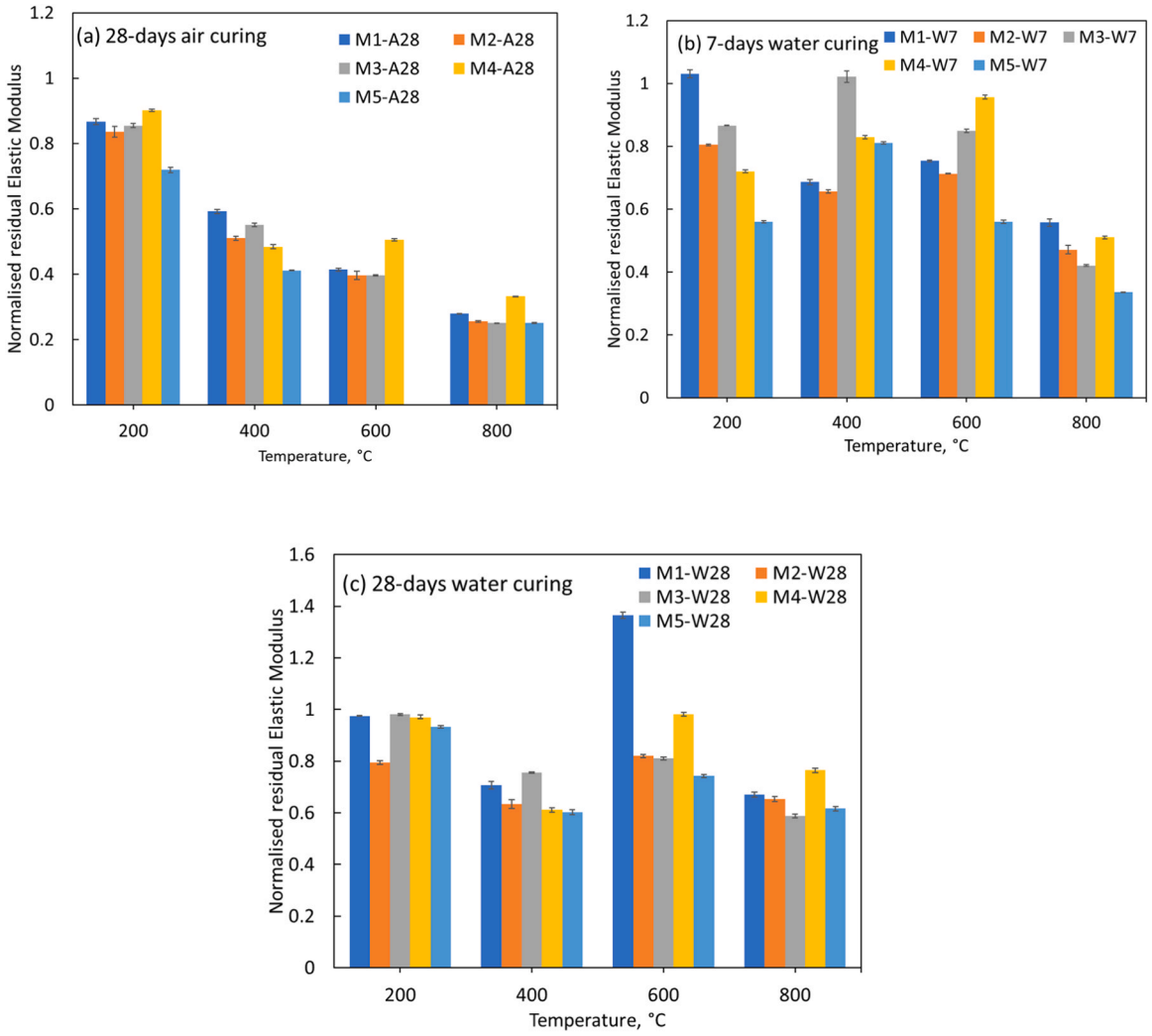

Fig. 6. Residual elastic modulus of HSECC specimens after elevated temperature exposure and (a) 28 days re-curing in air (b) 7 days re-curing in water (c) 28 days re-curing in water.

incorporation of slag may also promote the formation of mono-carboaluminates, and the decomposition of dolomite into CaO further increases rehydration product formation, potentially enhancing the recovery of compressive strength. It is worth noting that while M5 mix specimens showed significant strength recovery after water re-curing, their overall normalized strength remained lower due to the severe damage they underwent after thermal exposure. For example, at 800°C, 28-day water re-cured M4 specimens retained about 65 % strength. In contrast, M5 exhibited the lowest residual compressive strength among all mixes, retaining only 39 % of the original strength, indicating that silica fume-based mixes may not be favourable for fire-resistant applications.

3.3. Residual elastic modulus

Post-exposure curing is also found to have significant effect on the residual elastic modulus, and similar to the residual compressive strength, the extent of recovery is influenced by both the type of curing and the mix design.

3.3.1. Effect of type of re-curing

Consistent with the trend observed in residual compressive strength, specimens subjected to air re-curing showed minimal improvement in the residual elastic modulus after 28 days. For instance, the elastic modulus of M4 specimens exposed to 800°C was approximately 30 %, compared to 33.2 % in non-cured specimens (Fig. 5). Improvements in modulus were generally below 10 % across all mix types. In contrast, specimens re-cured in water exhibited significant recovery, particularly for those exposed to temperatures of 400°C and above. Notably, even a short re-curing period of just 7 days resulted in substantial increase. For specimens exposed to 400°C, the elastic modulus increased by 25–110 % compared to non-cured specimens. This improvement further increased to up to 124 % at 600°C and 104 % at 800°C, relative to the non-cured specimens. Since elastic modulus is more sensitive to microcracks and pore formation than compressive strength, its reduction at elevated temperatures is also considerably higher due to thermal-induced damage [23]. During rehydration, water penetration facilitates the filling of these micropores and cracks, leading to the formation of new hydration products. This process effectively restores the integrity of the matrix, resulting in increased stiffness and a more pronounced recovery in elastic modulus compared to compressive strength.

3.3.2. Effect of type of SCM

Expectedly, the type of SCM had significant influence on the elastic modulus recovery after re-curing as shown in Fig. 6. In case of mix M1, the elastic modulus retention in specimens exposed to 400°C increased from about 68.6 % after 7 days of water re-curing to 70.7 % after 28 days of re-curing. Specimens exposed to 600°C demonstrated an even

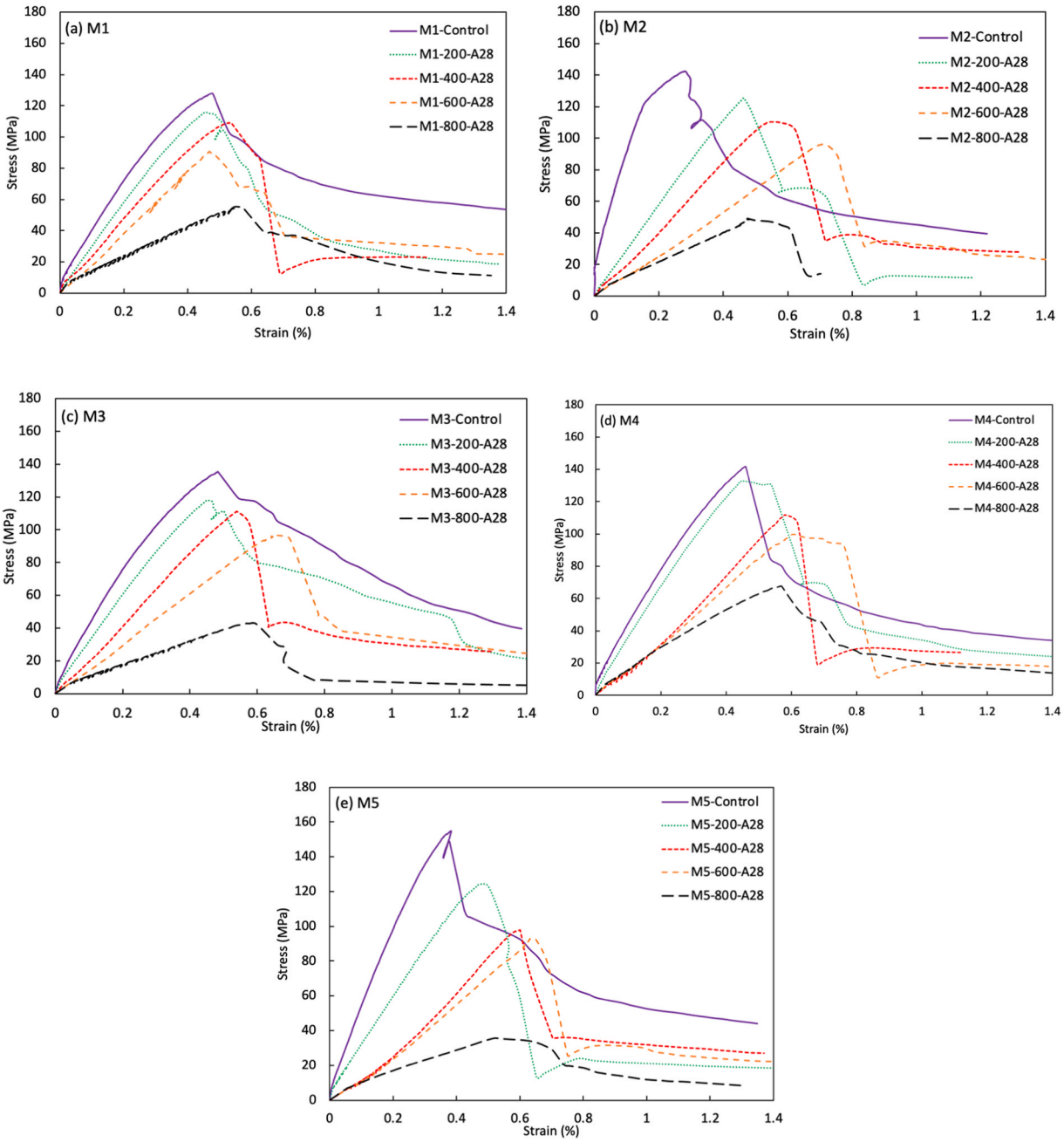

Fig. 7. Residual stress-strain response of HSECC mixes after 28 days re-curing in air (Note: Control refers to the specimens tested at room temperature before heating).

greater retention, reaching about 136 % of the control specimens after 28 days of re-curing. However, at 800°C, where the specimens experienced severe degradation, the modulus retention dropped to 67 %, though it still surpassed the retention observed in non-cured specimens (27.28 %). This reflects an increase in elastic modulus by 20 % to up to 233 % compared to air-cooled specimens at different temperature ranges.

A similar trend was observed for other mixes, with all exhibiting significant recovery, especially those exposed to higher temperatures. For instance, Mix M3, which contained 1.25 % PE fibre, demonstrated a recovery of 135 % for specimens exposed to 800°C, slightly lower than M1 specimens (145 % recovery). Both M4 and M5 mixes showed similar improvements, with modulus recovery of approximately 155 % compared to air-cooled specimens. It is important to note that while the recovery in elastic modulus was significant, the normalized modulus values still varied between mixes, particularly when comparing the water re-cured and air-cooled specimens.

In terms of normalized modulus, mixes M2, M3, and M4, which contained GGBFS or combinations of FA, GGBFS, and dolomite, showed retention at 28 days of around 81–98 % for 600°C-exposed specimens and around 58–76 % for 800°C-exposed specimens, with mix M4 showing the highest modulus retention among the three. The recovery in modulus was relatively lower in mix M5 specimens when compared to M1 or M4. M5 showed retention of 33.6 % for 800°C-exposed specimens after 7 days of water re-curing, which increased to 61.5 % after 28 days of re-curing. This indicates that the initial decomposition and behaviour under fire significantly influence the recovery of both strength and modulus. Therefore, though silica fume-based mixes exhibited a higher recovery rate, they initially suffered more severe degradation and hence, their properties remained at much lower levels than those of the GGBFS-

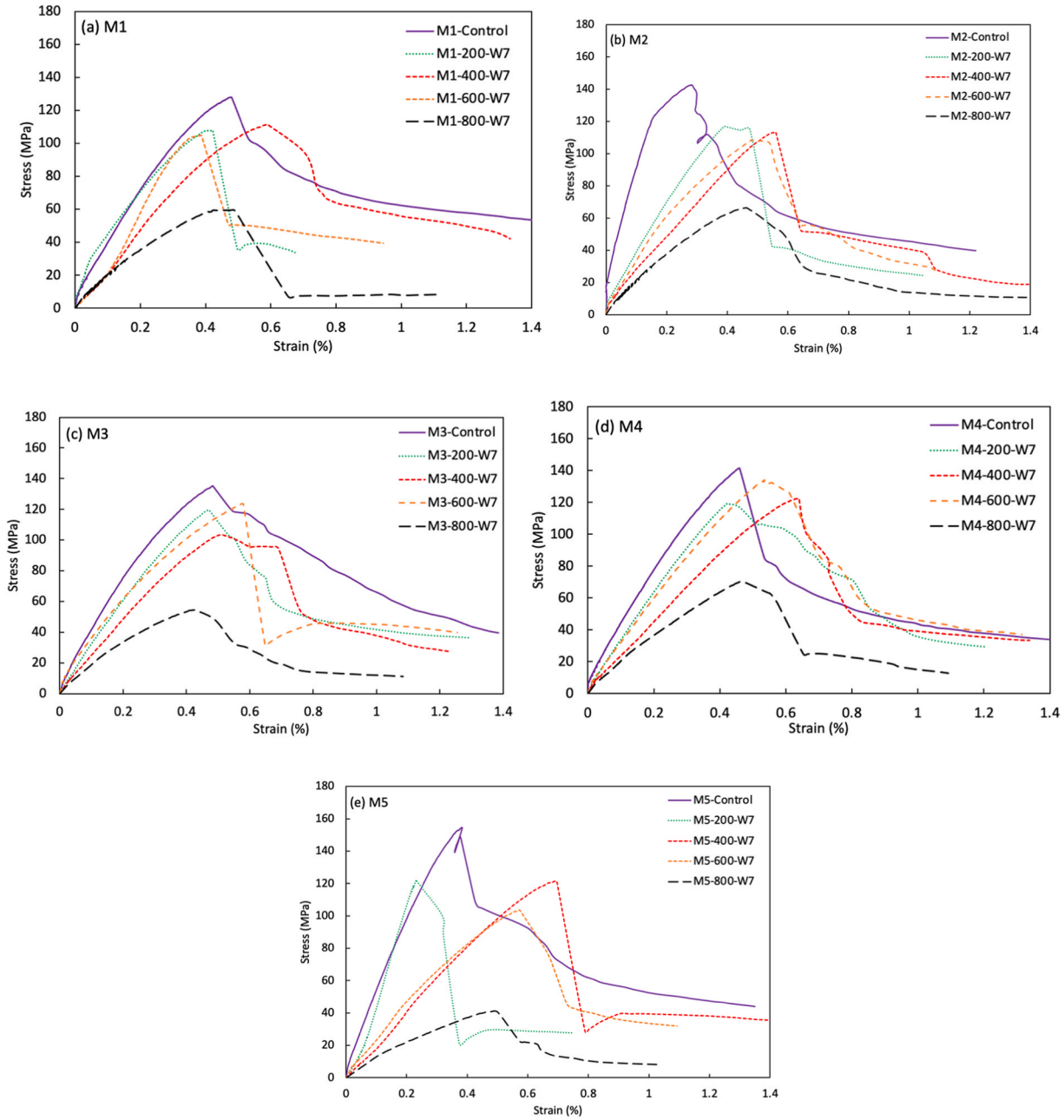

Fig. 8. Residual stress-strain response of HSECC mixes after 7 days re-curing in water (Note: Control refers to the specimens tested at room temperature before heating).

based mixes.

3.4. Stress-Strain relationship

In order to understand how post-exposure re-curing affects the stress-strain relationship and peak compressive strain, the compressive stress-strain behaviour of all five mixes was recorded at various post-fire curing stages for target temperatures of 200°C, 400°C, 600°C, and 800°C, as illustrated in Figs. 7 to 9. A comparison was made for different re-curing types, and the stress-strain curve at room temperature was plotted alongside to highlight the extent of improvement following re-curing. This analysis is essential for understanding the failure strain after matrix decomposition and the role of rehydration in modifying the peak strain.

3.4.1. Post-fire curing in air

The stress strain behaviour of the 28-days post-fire air cured specimens was fairly similar to the air-cooled samples (AC) for all types of mixes [18]. The stress-strain curves at each temperature and re-curing stage comprised of an elastic region followed by a parabolic section leading to peak stress and finally a descending section. In general, no significant improvement was observed from air re-curing. Compressive strength decreased with increase in temperature and the stress-strain response became increasingly flatter as expected (Fig. 7). Overall, the strength-strain response for air re-cured (A28) specimens remained similar to the air cooled (AC) specimens.

3.4.2. Post-fire curing in water

Strength improved with the post-exposure re-curing in water, and this was clearly visible in the stress-strain response as shown in Figs. 8–9. Compared to air-cooled or air re-cured specimens (Fig. 7), the

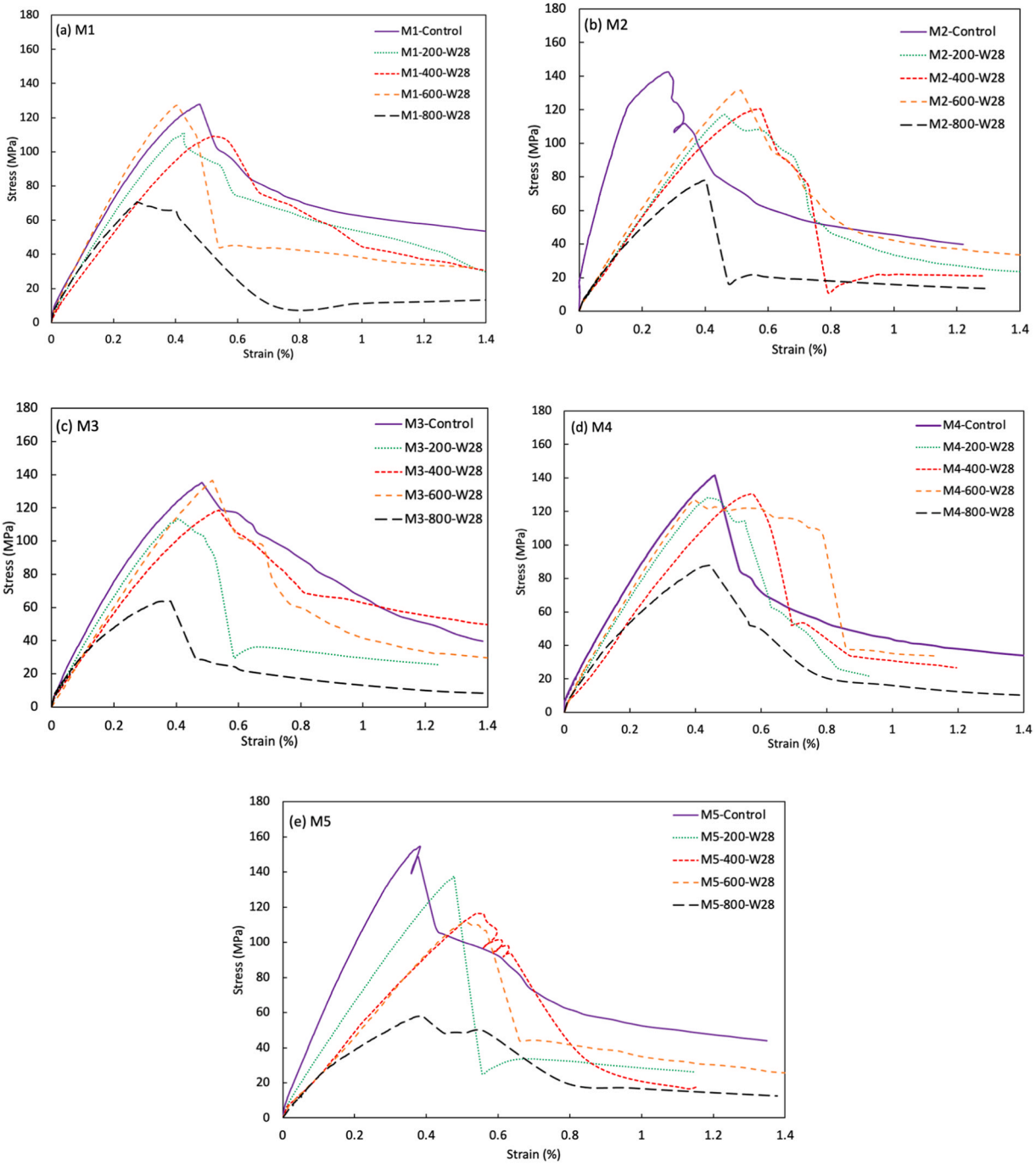

Fig. 9. Residual stress-strain response of HSECC mixes after 28 days re-curing in water (Note: Control refers to the specimens tested at room temperature before heating).

initial slope of the curves at all temperatures became steeper, resulting in increased stiffness and decreased peak compressive strain. With increase in temperature, the peak compressive strain decreased especially after 200°C. The lowest peak strain was observed in the 28 days water re-cured specimens, indicating that re-curing enhances the brittleness of the matrix regardless of the mix type. However, the extent of variation is influenced by the type of the matrix and fibre content as previously explained in Section 3.2.

Despite a significant variation in the stress-strain response of the water re-cured specimens, their failure pattern resembled the air-cooled specimens as shown in Fig. 10. Generally, the failure pattern in the control specimens was characterized by a fine, inclined shear crack running along the height of the specimen. As the exposure temperature increased, the crack width also increased. Beyond 400°C, this single crack pattern transitioned into multiple interacting cracks, likely due to the reduced fibre bridging, which contributed to the degradation of the matrix under higher temperatures.

3.5. Microstructural analysis

3.5.1. Post-fire curing in air

A general effect of re-curing in air can be assessed through the variation in specimen mass, as rehydration is expected to result in some mass gain. Fig. 11 illustrates the change in mass for M1 to M5 specimens across different temperature ranges after air cooling and subsequent re-curing in air for 28 days. The percentage change (mass gain) is expressed

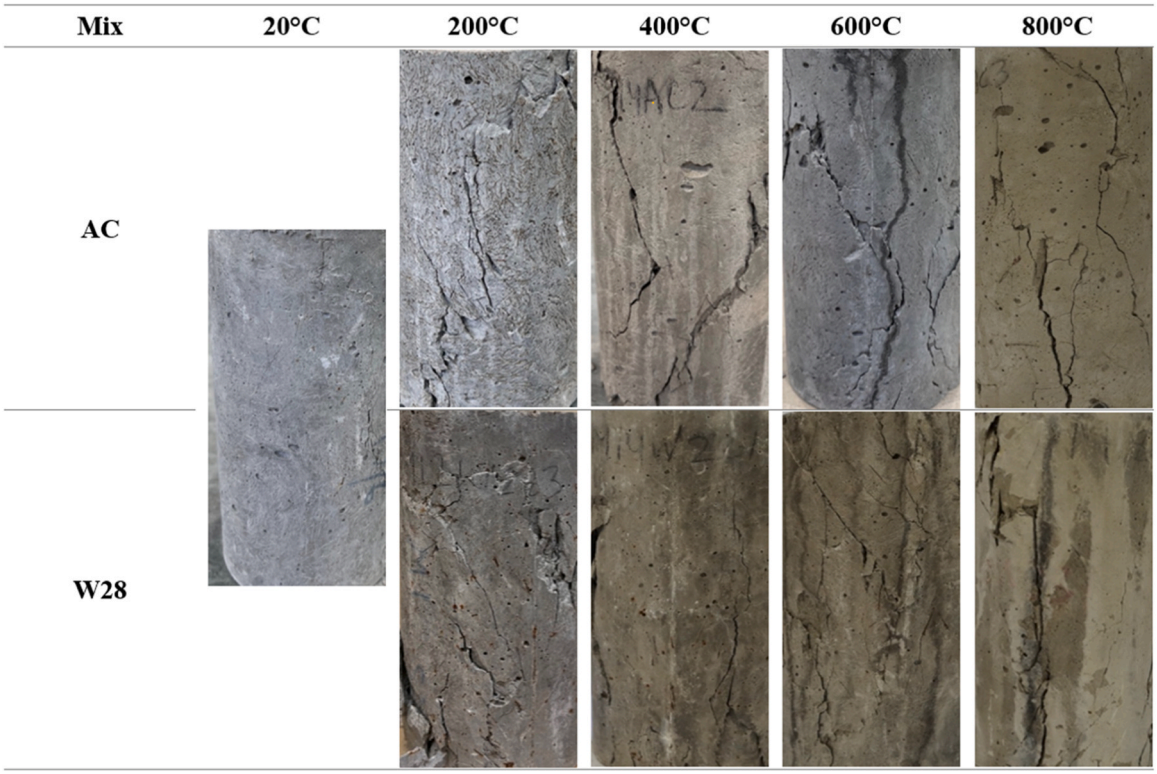

Fig. 10. Comparison of the failure pattern of M1 mix air-cooled and 28-day water re-cured specimens after compression testing.

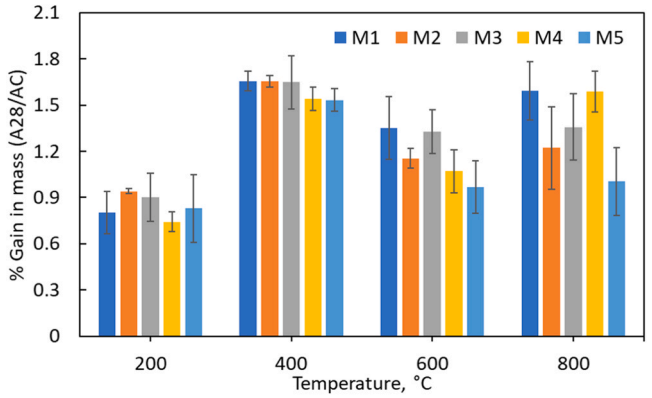

Fig. 11. Ratio of change in mass (mass gain) of HSECC mixes as a ratio of 28 days air re-curing and air cooling.

as the ratio of the mass of 28-day air re-cured specimens to the mass of air-cooled specimens.

As can be seen from the Fig. 11, there is negligible to very little gain in mass with air re-curing and the gain is generally higher (around 1–1.5 %) at higher temperature ranges. This slight increase in mass could be attributed to the absorption of moisture from the surrounding atmosphere, possibly initiating rehydration. However, there is no indication of improvement in density or further hydration other than the improvement in surface texture. This can be further confirmed through Fig. 12 which shows the SEM micrographs of the air re-cured 600–800°C exposed M4 and M5 mix specimens. The micrographs focus on vacant channels to detect any potential rehydration products. Results indicate that post-fire air re-curing did not cause significant microstructural change at 600°C, with no clear signs of rehydration. However, at 800°C, the M4 specimens showed a minor formation of platelet like crystals during air re-curing (Fig. 12c), potentially indicating the onset of hydration on the surface.

The comparison of X-ray diffractograms between 28-day air-cured specimens and air-cooled specimens further illustrates the limited effectiveness of post-fire re-curing in air under ambient conditions. Fig. 13 presents the XRD curves for M5 mix specimens exposed to 600°C. All peaks observed in the air re-cured specimens are also present in the air-cooled ones, with no indication of new hydration product formation. The peak intensities also remain largely unchanged, confirming that air re-curing under environmental conditions has minimal influence on the microstructure of HSECC specimens, irrespective of the matrix composition. This finding can be valuable for future studies that perform mechanical tests immediately after elevated temperature exposure. Since air curing has little effect on microstructural changes, researchers can focus on cooling the specimens to release internal pressure without compromising the accuracy of test results. This flexibility is especially advantageous when dealing with large batches of specimens exposed to elevated temperatures, allowing for a more flexible post-exposure testing timeline.

3.5.2. *Post-fire curing in water: formation of rehydration products*

3.5.2.1. SEM analysis. SEM analysis was performed to investigate the microstructural changes in HSECC specimens subjected to varying exposure and re-curing conditions. The analysis aimed to highlight the potential formation of rehydration products and their locations within the matrix. Figs. 14–16 depict the results of the SEM analysis of different HSECC specimens (M1, M4 and M5) subjected to various exposure and re-curing conditions. The micrographs in Fig. 14 illustrate the effects of air re-curing, water re-curing for 7 days, and water re-curing for 28 days on the M1 mix specimens exposed to 600°C. Vacant channels that formed as a result of fibre melting can still be observed in the SEM micrographs of the air re-cured specimen with no sign of rehydration (Fig. 14a).

The rehydration process was activated after the addition of water. This was confirmed by the presence of fibrous shaped C-S-H and needle

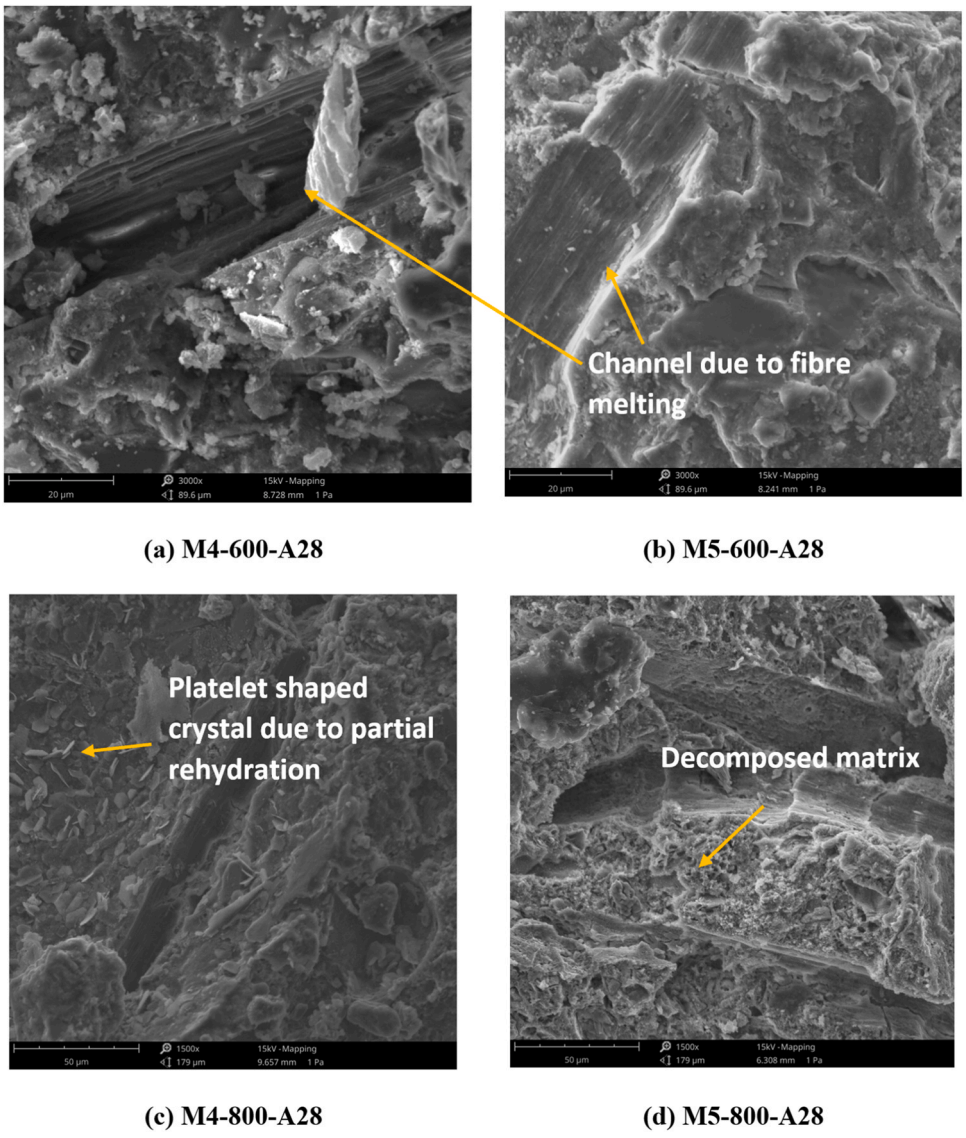

Fig. 12. SEM micrographs of 600–800°C exposed M4 and M5 specimens after air re-curing.

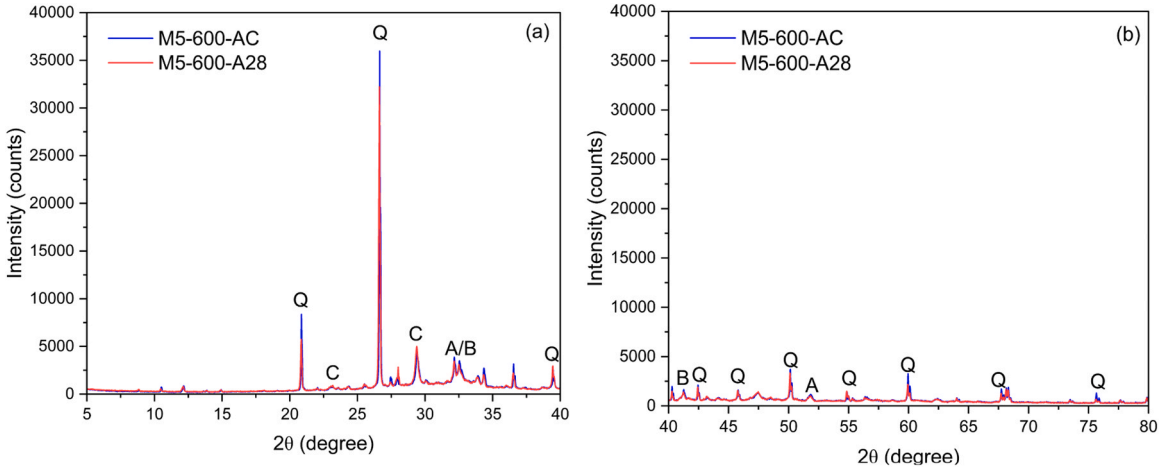

Fig. 13. Comparison of X-ray diffractograms of 600°C exposed M5 air re-cured and air-cooled specimens for (a) 5 – 40° 2θ (b) 40 – 80° 2θ.

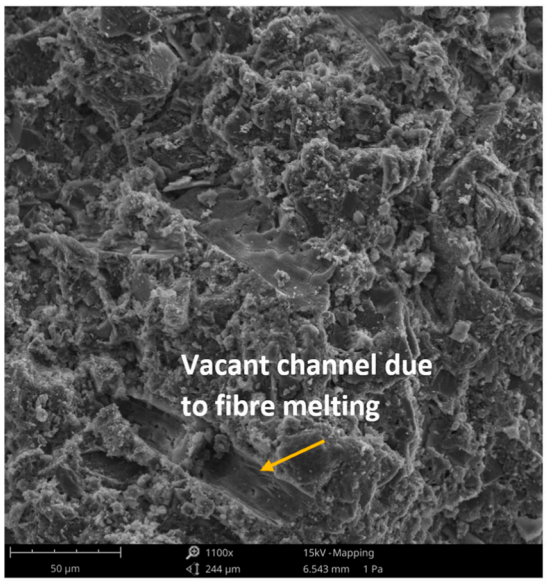

(a) M1-600-A28

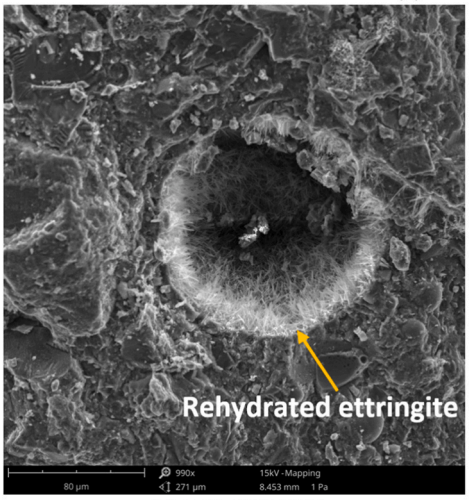

(b) M1-600-W7

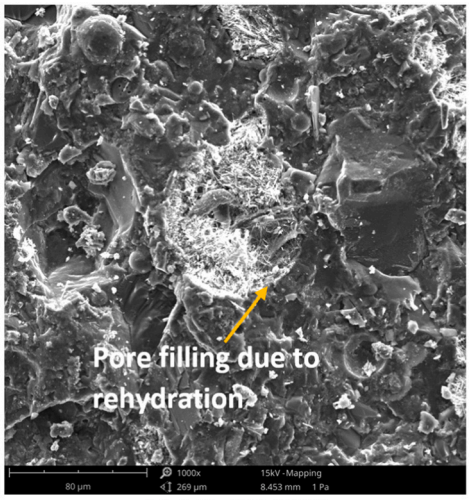

(c) M1-600-W28

Fig. 14. SEM micrographs of 600°C exposed M1 specimens after (a) air re-curing and (b/c) water re-curing.

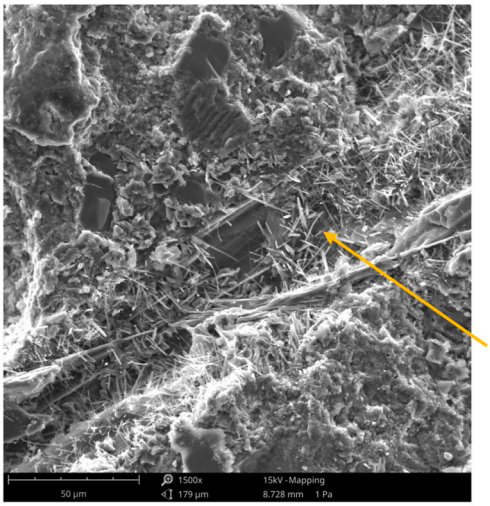

(a) M4-800-W7

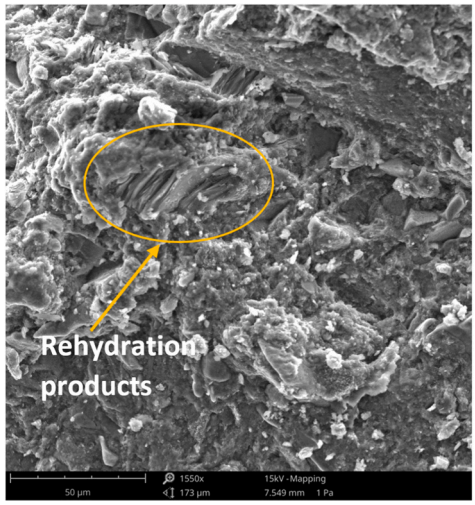

(b) M4-800-W28

Fig. 15. SEM micrographs of 800°C exposed M4 specimens after (a) 7-days and (b) 28-days water re-curing.

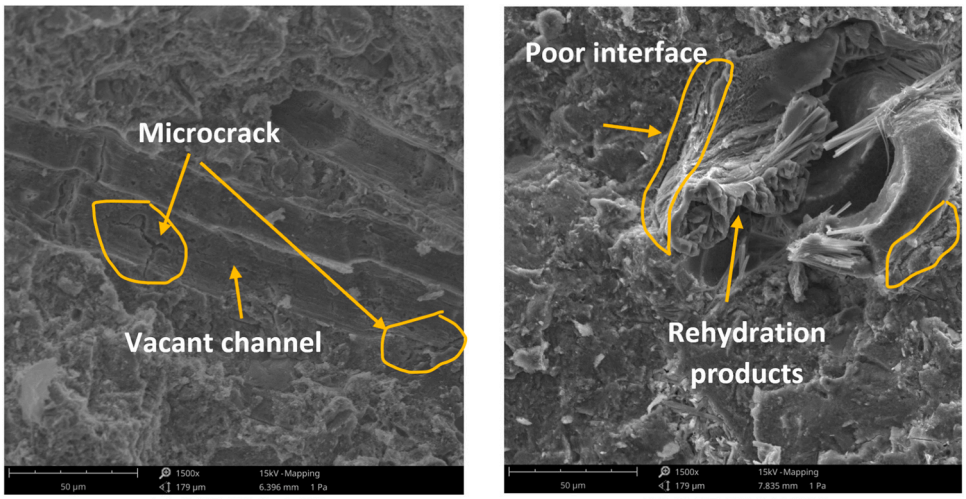

Fig. 16. SEM micrographs of 800°C exposed M5 specimens after (a) air re-curing and (b) water re-curing.

like ettringite found within cement micropores (Fig. 14b). Prolonged curing for 28 days led to a more extensive formation of these rehydration products, as shown in Fig. 14c. Rehydration products were observed to completely fill and densify the microstructure, reducing porosity and significantly contributing to the recovery of compressive strength. A similar pattern of microstructural changes was observed in the M4 mix specimens, as shown in Fig. 15. Both ettringite and portlandite were formed in the 800°C exposed M4 specimens during re-curing. It is clear that the rehydration led to filling of melted channels and wide pores inside the cementitious matrix, potentially leading to increase in strength.

Mix M5 also showed similar rehydration product formation. Fig. 16 compares the microstructure of M5 mix specimens exposed to 800°C after air re-curing and water re-curing. After air re-curing, the matrix (Fig. 16a, Fig. 12d) showed considerable degradation, characterized by a porous structure, microcracks, and decomposition by-products. However, following re-curing, the formation of rehydration products was observed which improved the compactness of the matrix and as a result, enhanced its strength.

In all the mixes, the rehydration products appeared to *sew* cracks and voids, contributing to the recovery in strength. However, the interfacial regions remained partially rehydrated (Fig. 15b). Restricted water access to deeper regions, likely due to capillary action, may have restricted the rehydration process. Additionally, heterogeneous decomposition might have resulted in variably reactive regions within the matrix, further limiting the effectiveness of recovery. These findings highlight the need for advanced characterization techniques to further analyse the inaccessible interfacial regions and better understand the mechanism for improving the microstructural recovery.

3.5.2.2. XRD analysis. Fig. 17 shows the X-ray diffractograms of M1 mix after exposure to 600°C and different re-curing stages. Only the diffractograms of mix M1 are presented to illustrate the general hydration phase change due to re-curing. The peaks of ettringite can be clearly seen at 9.08°, 15.80°, 22.12°, 24.25° in the water re-cured specimens (Fig. 17a) which were absent in the air-cooled specimen. Notably, the intensity of these peaks was higher after 28 days of re-curing compared to 7 days, indicating increased ettringite formation over time. Fig. 17(b) highlights several peaks of the unhydrated compounds which disappeared on water re-curing. Specifically, alite peaks at 30.71° and 33.57° and belite peak at 42.94° disappeared on water re-curing. This further confirms that the alite and belite may have reacted with water and other unhydrated pozzolans on re-curing to form new hydration compounds. Peak of Metajennite (Calcium hydrogen silicate hydroxide hydrate) has also become apparent at 45.05° in Fig. 17(b) confirming the presence of new hydration products as a result of water re-curing.

Similar phase change was also observed for 800°C specimens (Fig. 18). Ettringite peaks can be seen forming after water re-curing in Fig. 18(a) at 9.08° and 15.80°. In Fig. 18(b), the peaks of alite and belite were less intense especially in 28 days water re-cured specimens and new peaks of ettringite were observed with an overlap on alite. Peaks of belite also disappeared and instead, ettringite was seen forming as the new peak. This clearly indicates that water re-curing significantly changed the microstructure giving rise to several rehydration compounds which may have resulted in the strength improvement in all HSECC mixes, irrespective of the mix composition.

3.5.3. Post-fire curing in water: comparison of different blends

3.5.3.1. TG and DSC analysis. Fig. 19 presents the TG and DSC curves of the M1 mix after 7 and 28 days of water re-curing. Expectedly, the mass loss was higher in water re-cured specimens, reflecting the additional water absorbed during re-curing. Additionally, the mass loss between the 28-day and 7-day re-curing specimens differed significantly, reflecting the higher formation of rehydration products over time. For instance, the total mass loss at 800°C for the M1–600 specimens was 11.90 % when re-cured in water for 7 days, whereas it was 13.22 % after 28 days re-curing. The major difference between the TG curve of the water re-cured and the air-cooled specimens was in the first peak at around 105–110°C as it majorly represents the release of the free moisture. This continued till 220°C which also accounts for an additional decomposition of ettringite and hydrate water release from C-S-H indicating that extra C-S-H may be present in the water re-cured specimens.

These observations can be further corroborated by analysing the differential TG (DTG) curves of air-cooled and water re-cured M1 mix specimens, as shown in Fig. 20. It is well established that the mass loss till 200°C is primarily due to the dehydration of ettringite (AFt), monosulphates (AFm) and C-S-H, and this is followed by the dehydroxylation of calcium hydroxide (CH) in the range 350–500°C [5]. Fig. 20 indicates a clear difference between air cooled, 28 days air re-cured, 7 days water re-cured and 28 days water re-cured specimens due to the presence additional hydration products. The mass loss in M1–800-AC and M1–800-A28 between 120 and 220°C was 0.39 % and 0.31 %, respectively, indicating that air re-curing did not significantly contribute to the formation of new hydration products. In contrast, the mass loss increased to 1.56 % and 2.06 % for M1–800-W7 and M1–800-W28, respectively. This increase suggests the formation of additional

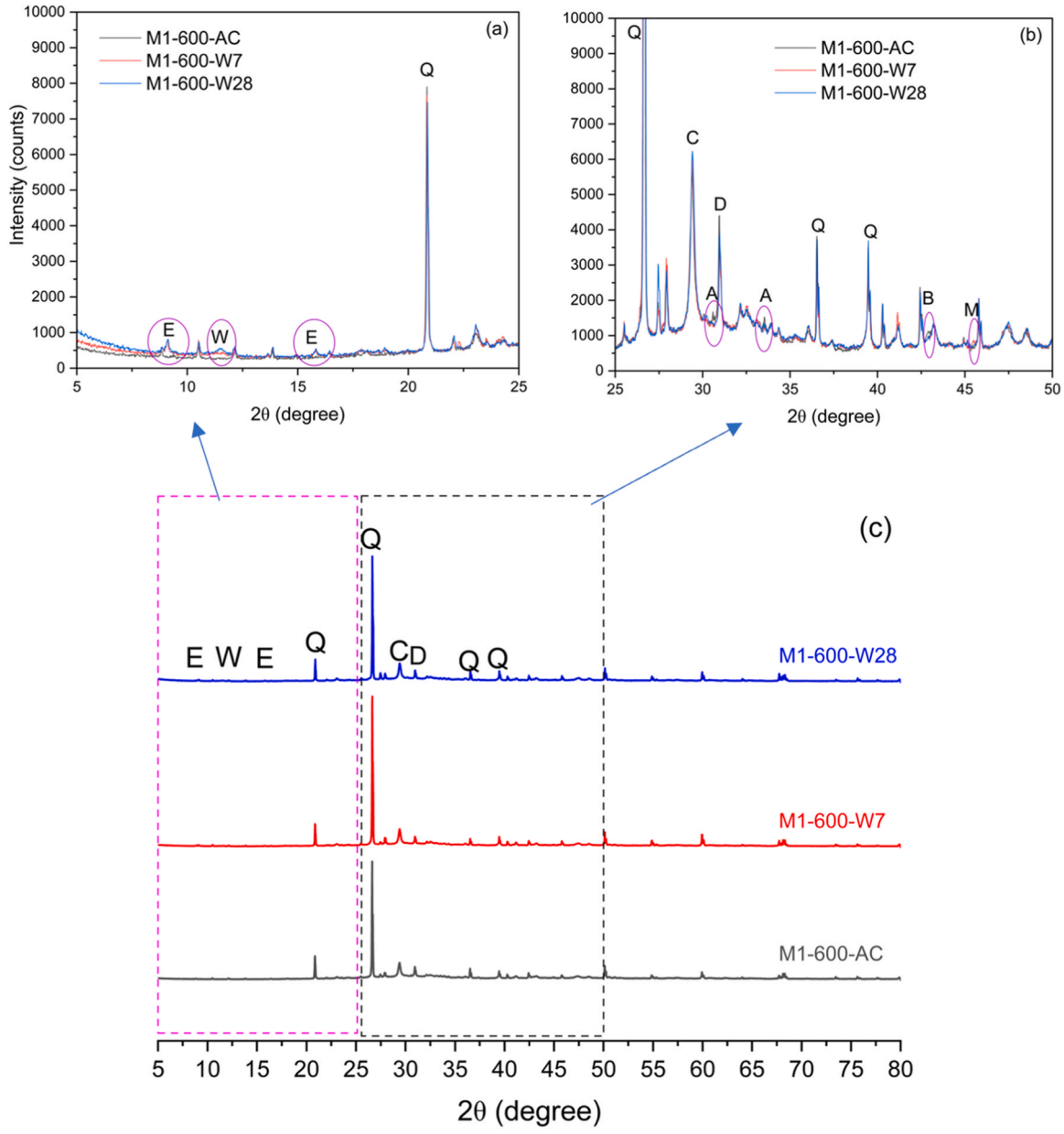

Fig. 17. Comparison of X-ray diffractograms of 600°C exposed M1 water re-cured and air-cooled specimens for (a) 5–25° 2θ (b) 25 – 50° 2θ (c) 5–80° 2θ [A – Alite, B – Belite, C- Calcite, D- Dolomite, E- Ettringite, M – Metajennite, Q – Quartz, W – Wollastonite].

hydration products, providing further evidence of the presence of C-S-H and other rehydration phases, which may have contributed to the observed strength improvement.

Fig. 21 shows the TG and DSC curves of M4 and M5 mix at 28-days of water re-curing. Similar to mix M1, the mass loss was found to increase due to the possible rehydration and absorption of free water and hence, the overall effect was similar to as observed for M1 mix. For instance, the mass loss at 800°C for M4–600 series was 10.06 % for 28-days re-cured specimens, whereas it was just 4.10 % loss for air cooled specimens.

If the DTG curves are compared, peaks generated due to re-curing can be clearly distinguished (Fig. 22). There was a clear peak between 100 and 200°C which may have been due to the release of free water and dehydration of C-S-H as explained above. The mass loss for the M4–600-AC specimens was approximately 0.22 % in this range, whereas it increased to 3.2 % for the M4–600-W28 specimens. Additionally, the mass loss between 400 and 500°C was 0.7 % for the M4–600-W28 specimens, compared to 0.25 % for the M4–600-AC specimens. This is further supported by a small peak around 460°C in the DSC curve for the M4–600 series, likely due to the decomposition of portlandite, suggesting that additional portlandite may be present in the 28-day water re-cured specimens (Fig. 21b). However, no significant difference in mass loss was observed beyond this range (2.44 % vs. 2.41 % between 600 and 800°C), indicating no additional presence of carbonates. Similar effect was noted for 800°C specimens. If compared with M1–800°C exposed specimens which had 4 times increase in mass loss between 120 and 220°C after 7-day re-curing and 5.3 times increase after 28-day re-curing, the effect was more evident for M4 mix. M4 mix underwent 6.5 times increase after 7-day water re-curing and 7.7 times after 28 days water re-curing, indicating a greater recovery potential, which may have contributed to the improved strength at this temperature.

The DTG peaks of the 600°C and 800°C exposed air-cooled and water-cured M5 mix specimens, as shown in Fig. 23, also clearly highlight the occurrence of rehydration. The initial range between 110 and 220°C showed a similar increase in mass loss. Mass loss for the M5–600-AC specimens was approximately 0.11 % in this range, whereas it

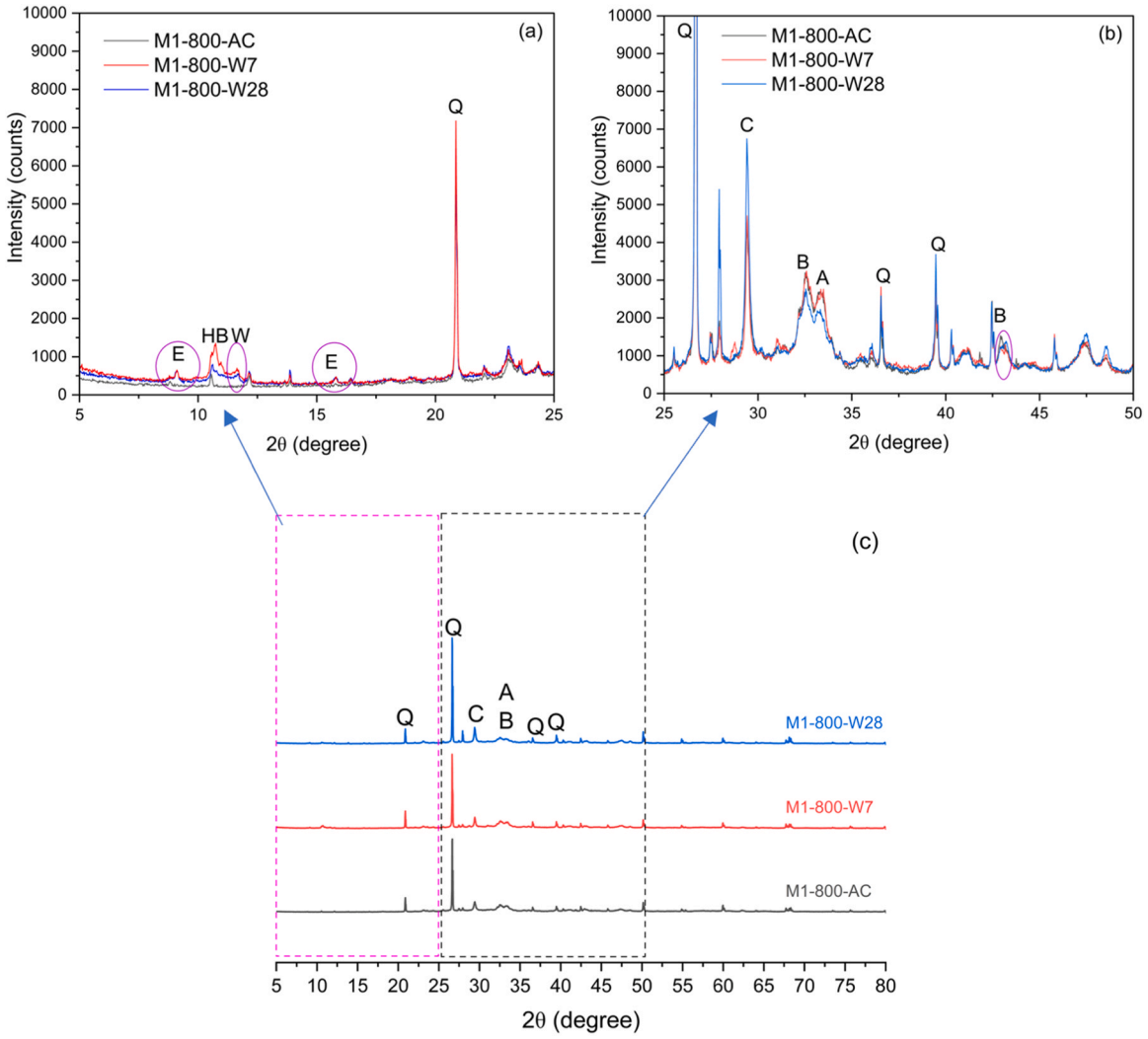

Fig. 18. Comparison of X-ray diffractograms of 800°C exposed M1 water re-cured and air-cooled specimens for (a) 5–25° 2θ (b) 25 – 50° 2θ (c) 5–80° 2θ [A – Alite, B – Belite, C – Calcite, E- Ettringite, HB – Hornblende, Q – Quartz, W – Wollastonite].

increased to 3 % for the M5–600-W28 specimens. Additionally, the M5–800-W28 specimens exhibited several peaks in the DSC analysis, particularly in the 400–500°C and 700–800°C ranges, as opposed to the flat curve observed in the air-cooled specimens (Fig. 21d). This suggests the presence of additional portlandite and carbonates in the M5 series, which differentiate it from M1-M4 mixes. In terms of percentage increase in the mass loss between 120 and 220°C, M5–800°C specimens underwent 7.5 times, and 14.7 times increase after 7 and 28-day re-curing indicating the highest recovery in terms of rehydration, as also reflected in the compressive strength results. This demonstrates the significant potential of silica fume-based cementitious matrix. However, despite this higher recovery rate, the damage these mixes sustained was considerably high and hence, the residual strength after re-curing still remained at the lower end for M5. This will be further confirmed through porosity analysis.

3.5.3.2. Porosity analysis. Pore size distribution for the samples before and after post-fire curing was analysed using the pore volume vs pore diameter curves obtained through MIP to understand the effect of different SCMs. To distinguish the characteristics of the distribution, five distinct pore size ranges were established as follows: (a) Gel pores (< 10 nm), (b) Transitional pores (10–100 nm), (c) Capillary pores (100–1000 nm), (d) Macro pores (10^3 – 10^5 nm), and (e) Surface conformance (> 10^5 nm). Previous studies suggested that it is difficult to avoid the surface conformance effect in MIP measurements due to the cracks and flaws on the specimen surface and these can also be introduced during sample preparation stage [24]. Therefore, this range was excluded from comparison to minimize potential errors.

Fig. 24 shows the pore size distribution of the M1, M4 and M5 mix specimens after exposure to 600°C. It can be observed that the macropores at 1.3 × 10^4 nm were highest in M5 mix and the lowest in the M1 mix. M5 exhibited a broad range for macro pores, encompassing all pore sizes within the range. On the other hand, both M1 and M4 samples lacked any pores within 10^3 to 5 × 10^3 nm. This trend of larger pore sizes in M5 continued through the capillary and transitional pore range, whereas M1 had higher pore sizes only in the gel pore region. The observed higher pore sizes in M5, followed by M4 and M1, support the mechanical performance trend at this temperature, with M5 exhibiting the poorest performance. The increased porosity in the M5 mix indicates a compromised microstructure, likely resulting from significant decomposition and degradation of the matrix.

Fig. 25 shows the comparison of M1 specimens at 600°C and 800°C before and after post-fire curing. As observed in Fig. 25(a), a significant shift in pore size distribution occurred with an increase in temperature. At 800°C, there was a marked increase in both macropores (around 1.1 × 10^4 nm) and pores below 1 micron, confirming the negative role of temperature rise on HSECC. Specifically, in the transitional pore region, M1–800-AC displayed a three-times higher pore volume compared to

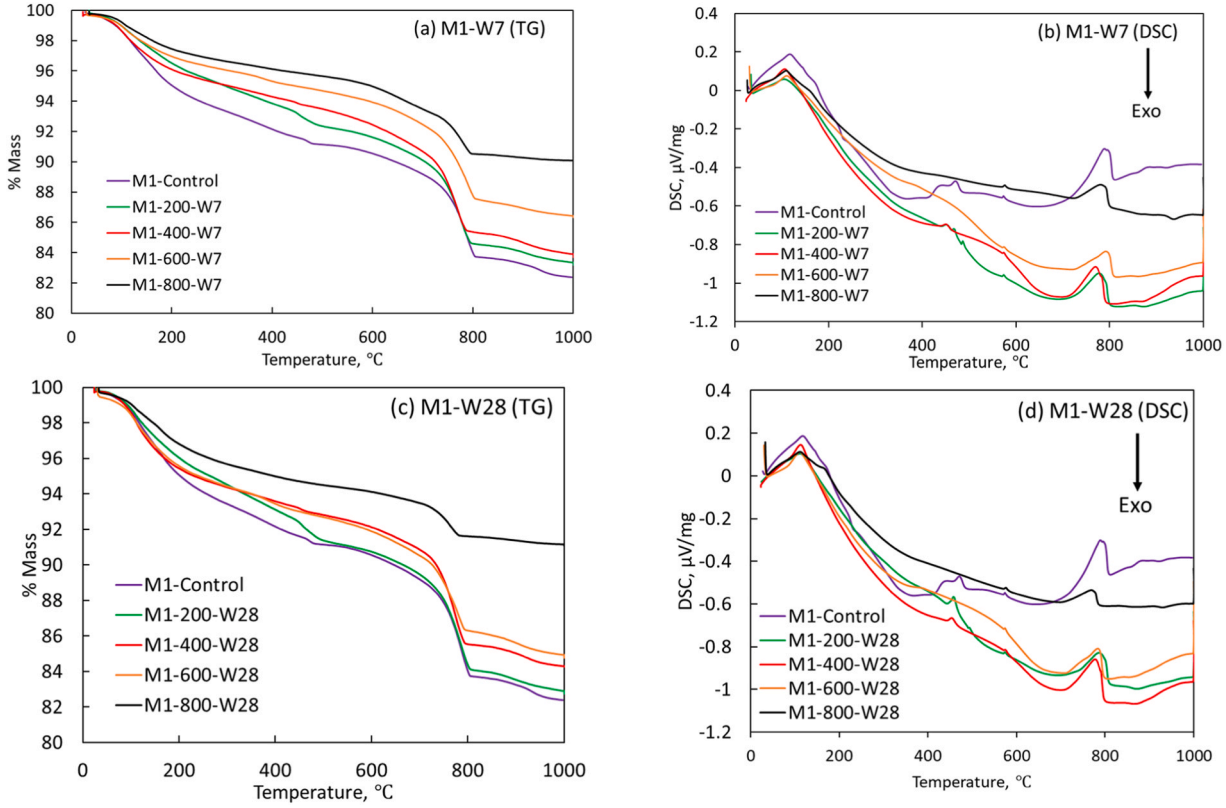

Fig. 19. TG (a,c)/DSC (b,d) curves of M1 specimens after 7-days and 28-days re-curing in water.

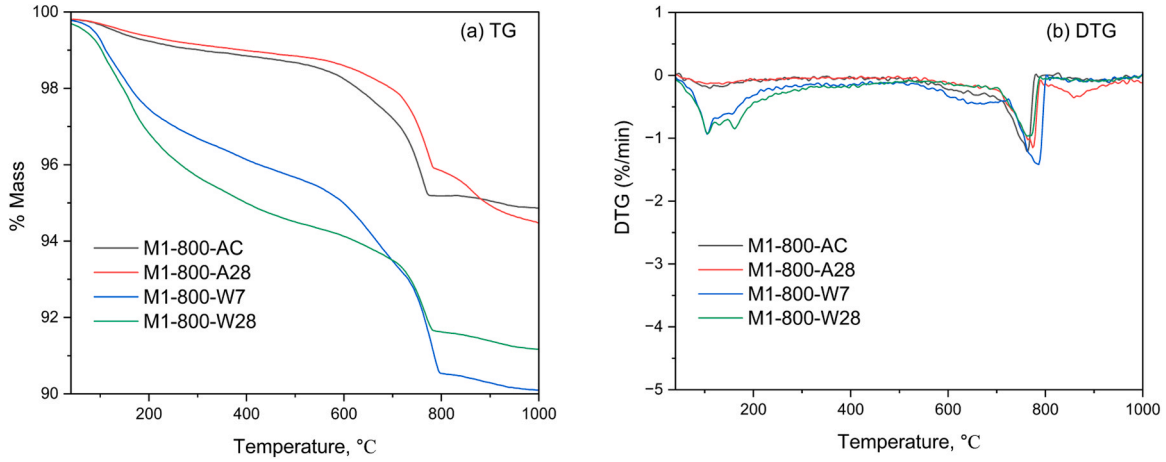

Fig. 20. (a) TG and (b) DTG curves of M1 specimens after exposure to 800°C.

M1–600-AC, with peak pore volume rising from 0.004 mL/g at 600°C to 0.014 mL/g at 800°C. Moreover, the pore volume in the capillary region was approximately twice as high for M1–800-AC compared to M1–600-AC, further highlighting the detrimental effect of temperature rise on the denseness and strength of mix M1.

Following post-fire curing, a refinement in pore size distribution was observed, accompanied by a reduction in macropores. The pore size refinement further improved with increase in the curing duration as shown in Fig. 25(b). For the 600°C-exposed specimens, the primary refinement occurred in the macro pore range (~14 microns), where the pore volume reduced from 0.002 mL/g to negligible levels. This reduction was accompanied by an increase in the pore volume of smaller-sized micro pores (~1 micron), suggesting a redistribution of pores as macropores were progressively filled with rehydration products. Comparing the 7-day and 28-day water-cured specimens, the 28-day curing resulted in a more substantial reduction in pore size. Transitional pores were reduced to a range of 1.5–2.5 microns after 7 days, with further refinement to 1–1.3 microns after 28 days. For 800°C-exposed specimens, a bimodal pore size distribution was observed with significant pore volume lying in macro pore (3–20 microns) and capillary-transitional pore region (0.03–1 microns) which corresponds to dehydration products and microcracks respectively. The peak with pore size centred at 0.2 µm is associated with pore structure coarsening of C-S-H hydration products, whereas the other nearby peaks might be the result of microcracking. This pore size noticeably reduced after water re-curing for 28 days with no micropores visible in the above stated range. Furthermore, the main peak in the transitional-capillary pore range shifted from 0.03–1 µm to 0.004–0.03 µm, indicating that

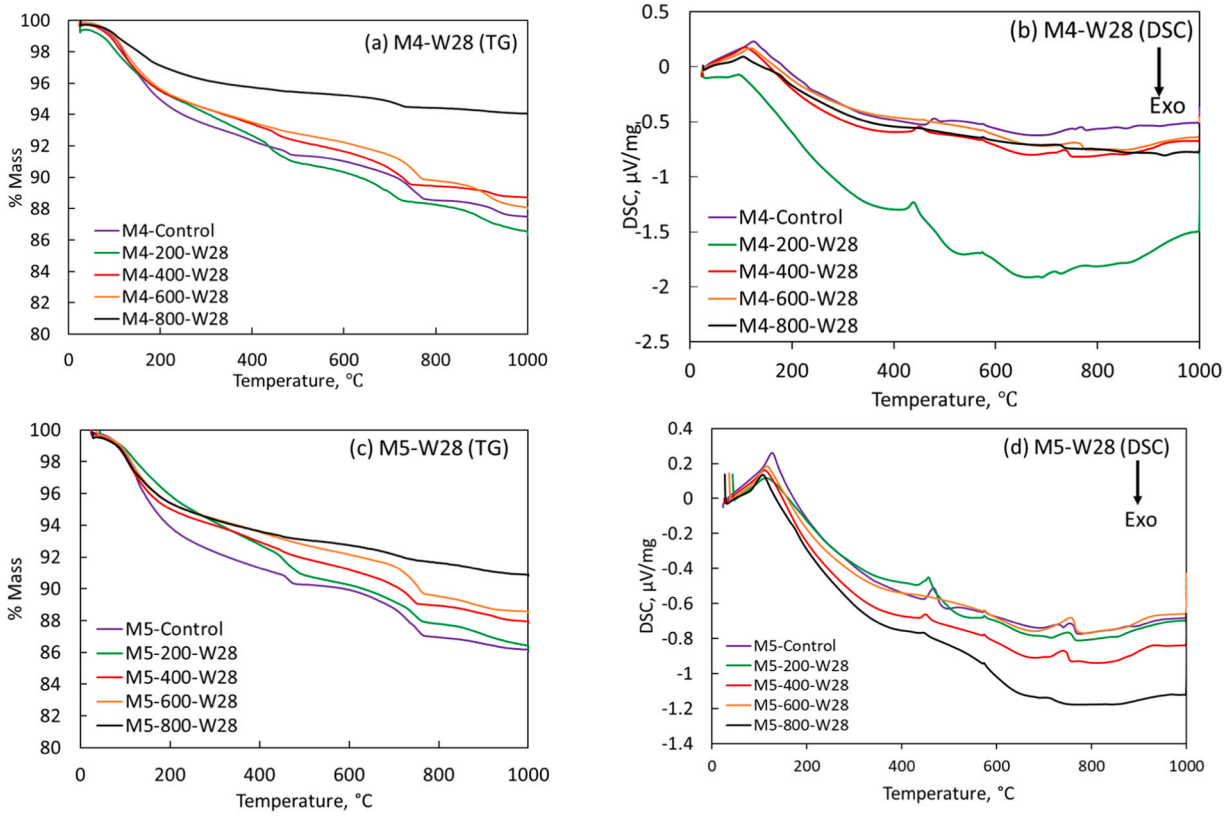

Fig. 21. TG (a, c) /DSC (b,d) curves of M4-M5 specimens after 28-days re-curing in water.

these pores were partially filled with newly formed rehydration products. This shows that micropores were healed during post-fire curing along with pore size refinement which may have led a significant rise in strength and stiffness of matrix. Pore refinement was more evident in 28 days cured specimens in comparison to 7-day cured specimens further confirming the importance of curing duration.

A similar trend in pore size distribution before and after post-fire curing was observed for M4 and M5 specimens. As shown in Fig. 26, 600°C-exposed M4 and M5 specimens showed significant volume of macro pores (1.4×10^4 nm) and irregular pore distribution for pore size lesser than 100 nm after exposure to 600°C. The macropores significantly reduced and pore refinement occurred after undergoing post-fire re-curing for 28 days. For instance, in M4 specimens, the pore volume corresponding to 14-µm pores decreased from 0.003 mL/g to nearly one-tenth of the original value (3×10^{-4} mL/g) after 28-day water re-curing. Similarly, while M5 specimens initially had a higher pore volume at 0.005 mL/g for the same pore size (indicating possibly lower strength), it also reduced to 4×10^{-4} mL/g after re-curing. This was due to the rehydration generating new hydration products which may have occupied the pore space effectively reducing the pore size.

When comparing the pore behaviour among M1, M4, and M5 specimens, mix M5 exhibited a broader range of macropores (1–7 microns) even after 28 days of water re-curing, with a pore volume of approximately 0.002 mL/g (Fig. 26c). In contrast, M1 specimens displayed smaller macropores (~1 micron) with a pore volume of 0.003 mL/g, while M4 specimens had the most refined pore structure, with macropores reduced to nearly negligible levels. This indicates that while the recovery process was observed in all HSECC mixes, M4 underwent a more pronounced transition toward the gel and transitional pore regions. This refinement in pore structure likely contributed to the highest normalized compressive strength in M4 at this temperature range.

4. Discussion on the effect of post-fire curing and rehydration

In the HSECC, the degradation from thermal exposure can manifest in several ways, including fine cracks due to thermal stresses, channels formed by polymer fibre melting, and the chemical decomposition of hydration products. Fig. 27 illustrates the general changes observed in HSECC after exposure to high temperatures and re-curing.

The decomposition and rehydration processes can be divided into two distinct temperature ranges–

- *100°C-300°C:*
  Ettringite decomposition and C-S-H dehydration occur within this range. In some cases, there may be a strength increase due to the increase in surface van der Waals forces between C-S-H molecules as a result of dehydration or due to the accelerated hydration caused by heating. However, in ECC, the melting of fibres may create voids, leading to a loss in strength. Therefore, the overall effect is determined by the balance between these opposing factors. Though rehydration is possible when exposed to water during re-curing [9], present study confirmed that the water infiltration for the 200°C-exposed specimens could potentially lead to reduction in the overall compressive strength. This reduction was likely caused by water entering capillary and gel pores, which weakens the C-S-H structure or triggers the depolymerization of silicates in C-S-H [20–22]. The trend during this stage was consistent across all HSECC mixes, irrespective of binder composition, indicating that strength reduction compared to room temperature specimens is a likely phenomenon.
- *300°C-800°C:*
  C-S-H (or C-A-S-H) decomposes to C_nS between 400 and 800°C [25,26]. These dehydrated products can rehydrate back to C-S-H (or C-A-S-H) and AFt with the presence of water during post-fire-curing. In addition, CH dehydrates to CaO from 350°C to 550°C and $CaCO_3$

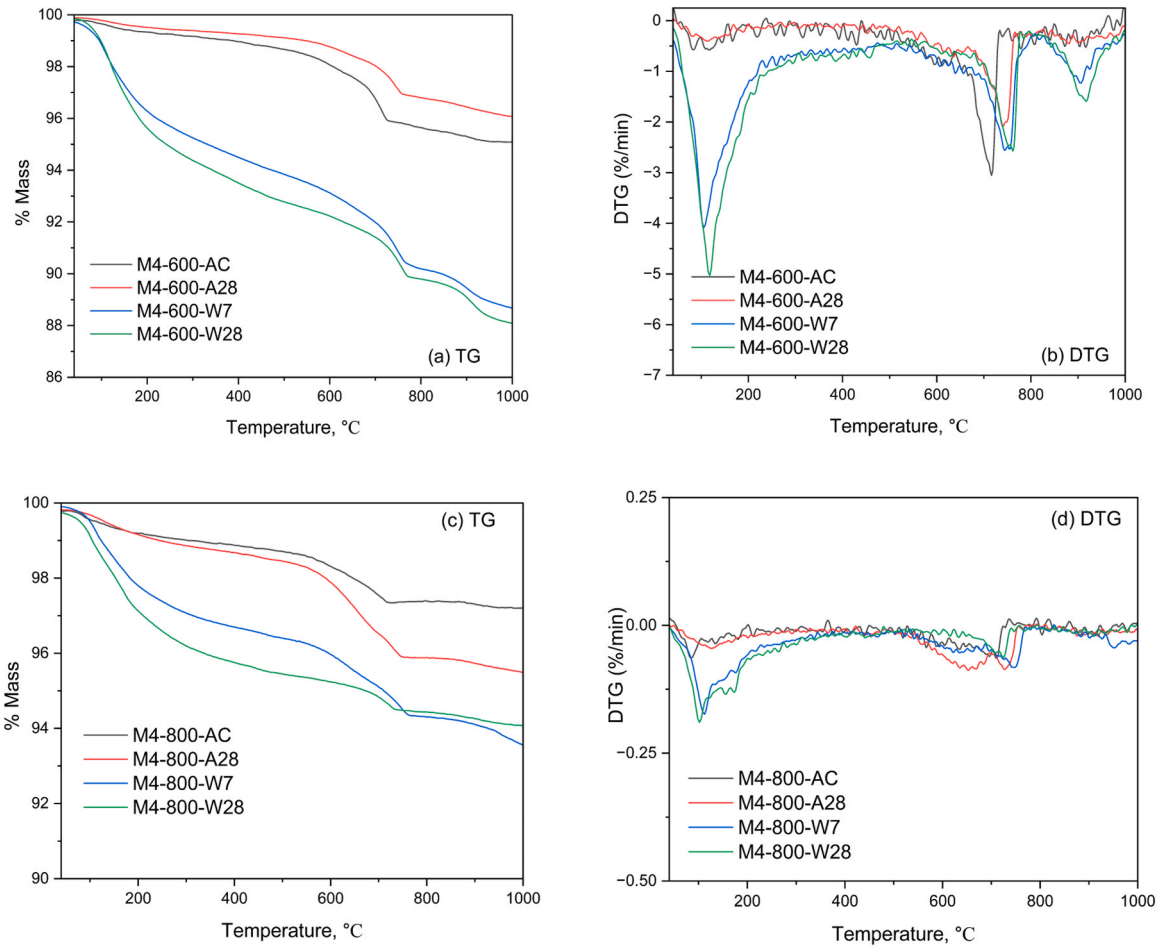

Fig. 22. (a/c) TG and (b/d) DTG curves of M4 specimens after exposure to 600°C and 800°C.

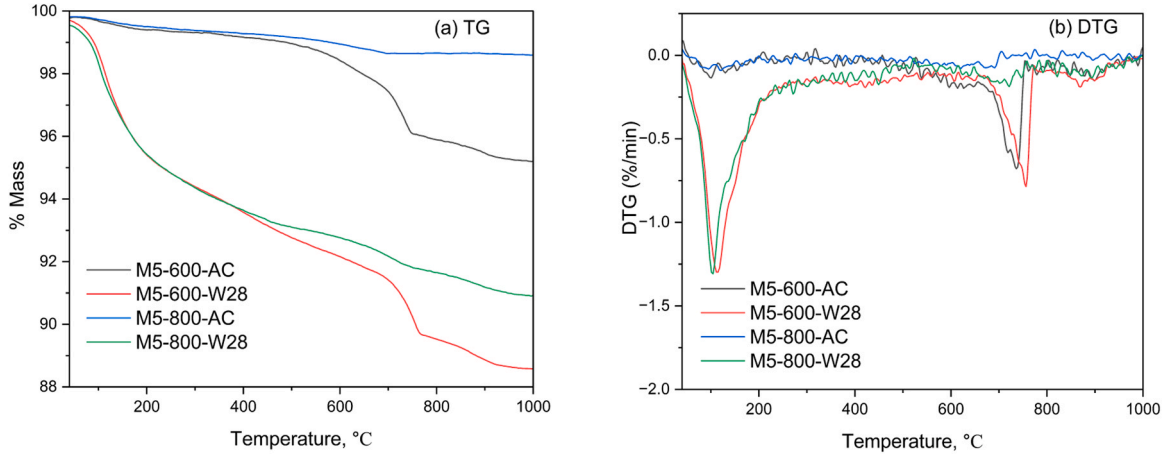

Fig. 23. (a) TG and (b) DTG curves of M5 mix after exposure to 600°C and 800°C.

decomposes to CaO beyond 650°C [27–29]. This CaO may participate in rehydration forming C-S-H and CH or may also carbonate back to $CaCO_3$ in the presence of atmospheric CO_2 [30–32]. It is important to note that the rehydration of CH and ettringite tends to cause volume expansion and can lead to additional damage to the matrix. However, in HSECC, the rehydration products can be accommodated in the additional space and interconnected channels formed by the melting of polymer fibres as confirmed by SEM micrographs.

Present study further demonstrated that the recovery in this range could be considerable but depends on the state of the specimens after thermal exposure. For specimens with significant degradation—caused by lower PE fibre content (leading to higher pressure buildup as seen in mix M3) or a dense matrix (e.g. silica fume based, Mix M5)—recovery is more complex and may even surpass that of less damaged matrix (M1, M2, and M4), depending on the extent of space created by minor cracks or the type of matrix (e.g., silica fume-based mixes may have more nucleation sites). However, the

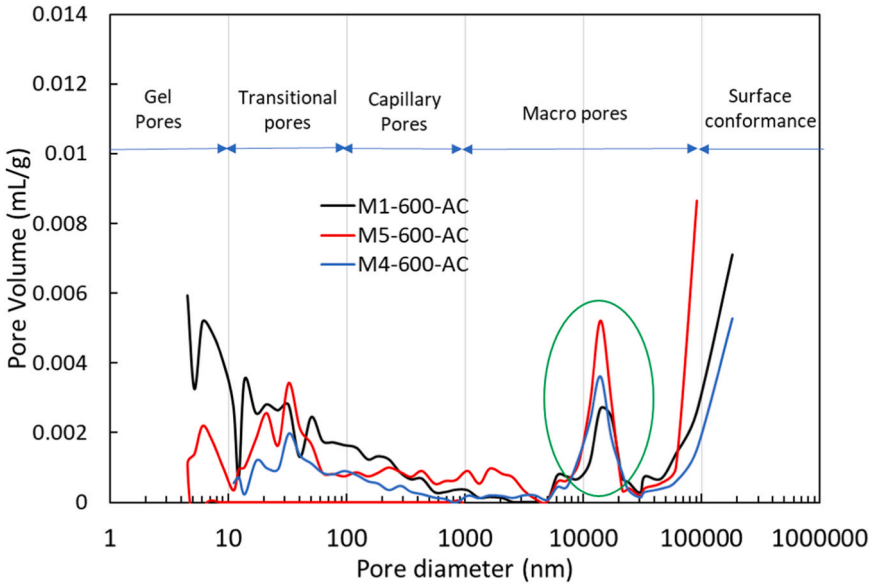

Fig. 24. Pore size distribution of M1, M4 and M5 specimens after exposure to 600°C.

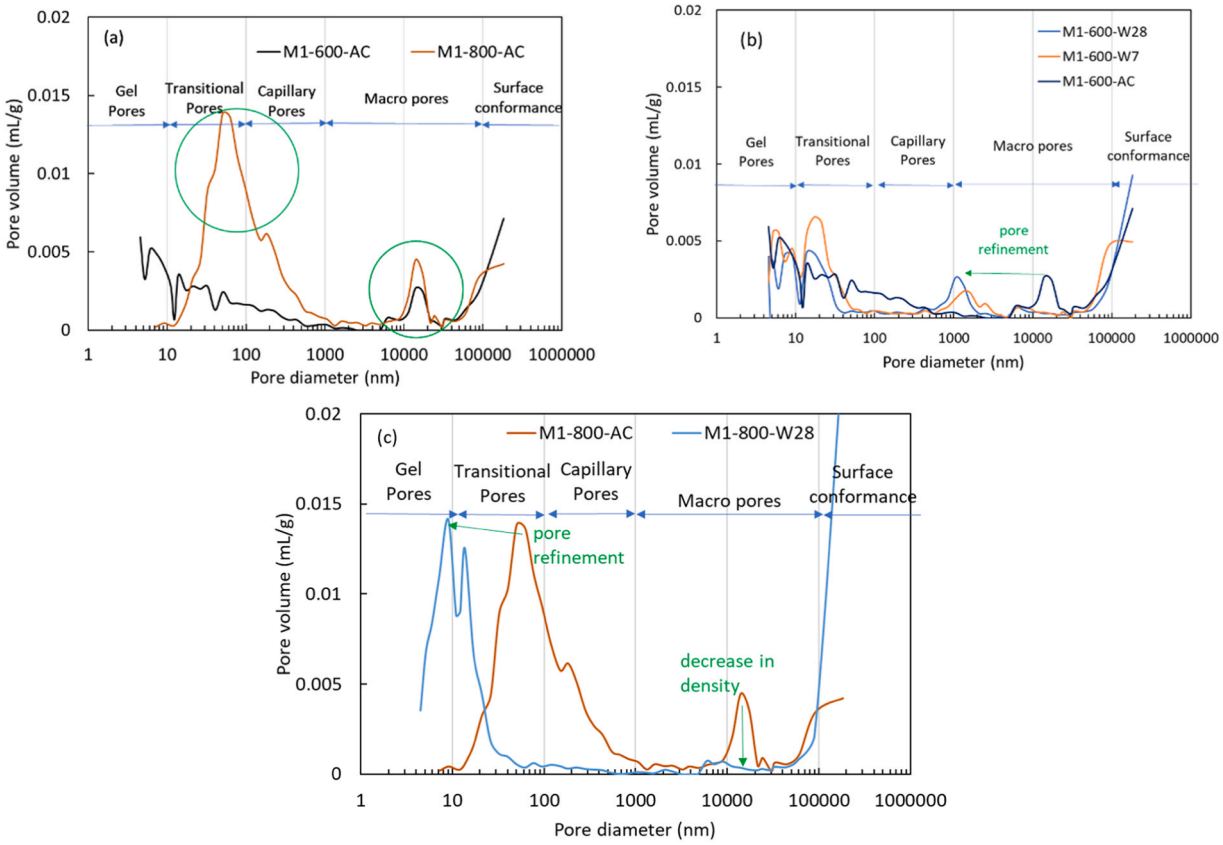

Fig. 25. Pore size distribution of M1 specimens (a) comparison between 600 and 800°C exposed specimens (b) effect of water re-curing duration in 600°C exposed specimens (c) effect of water re-curing in 800°C exposed specimens.

overall strength after recovery may remain still lower, especially at 600°C-800°C. At 400°C, decomposition is not yet complete for most hydrated products, recovery rate becomes highly variable as it is influenced by multiple factors, particularly the decomposition of PE fibres, and bonding of steel fibre with the matrix.

Overall, the formation of rehydration products and their associated effects depend on three key factors: the extent of matrix damage after thermal exposure, the availability of rehydration sites, and the space available to accommodate newly formed compounds. Higher exposure temperatures can result in more products available for rehydration. Moreover, a higher binder content offers more rehydration sites, and the voids created by melting polymer fibres provide additional space for hydration products, further improving the recovery process. However,

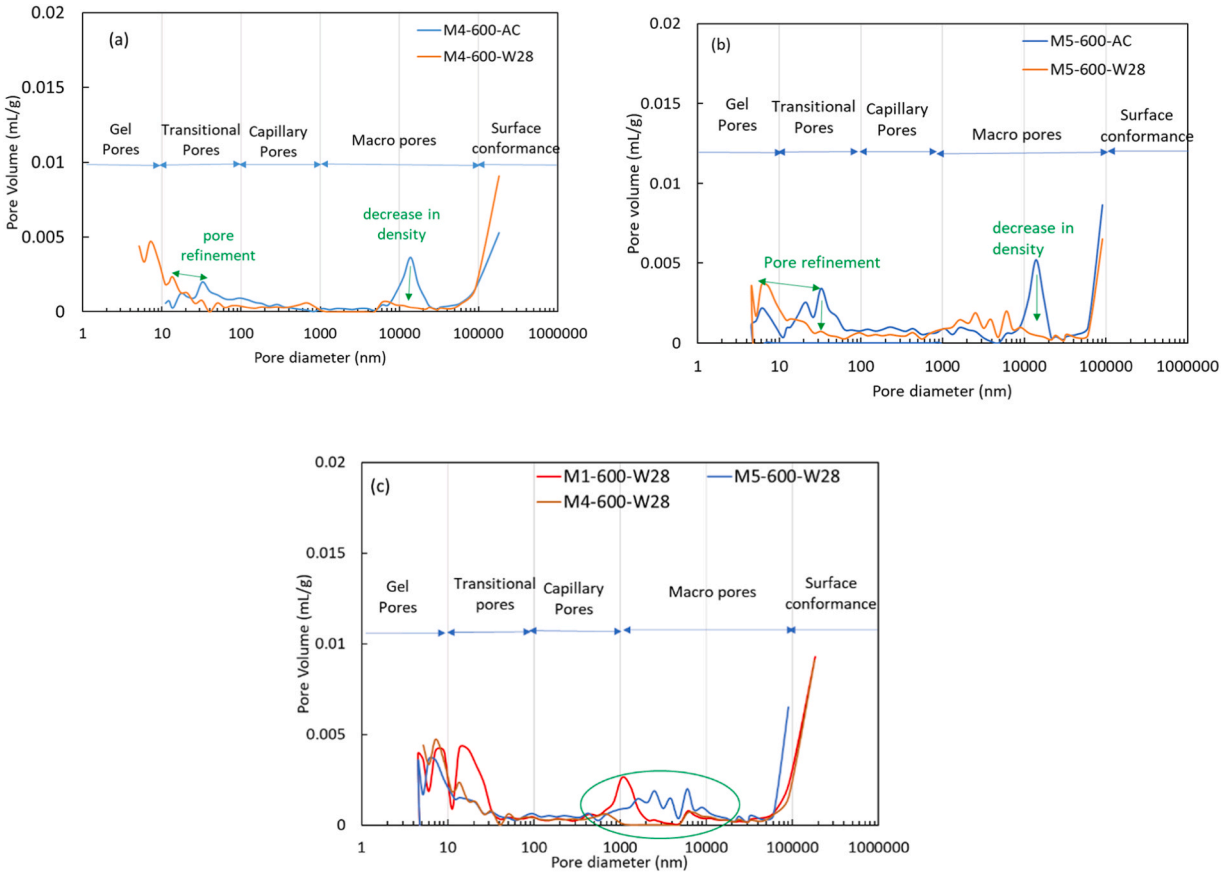

Fig. 26. (a) Effect of water re-curing in 600°C exposed M4 specimens (b) Effect of water re-curing in 600°C exposed M5 specimens (c) Comparison of pore size distribution of 600°C exposed M1, M4 and M5 specimens after water re-curing.

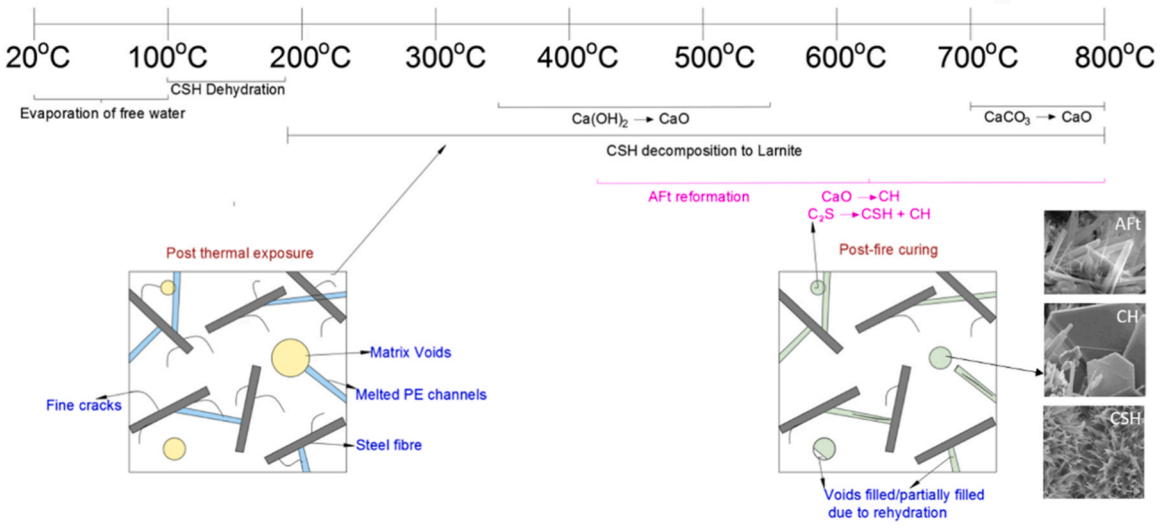

Fig. 27. Changes in HSECC after exposure to high temperature and subsequent re-curing.

the overall recovery depends significantly on the composition of the matrix. Mixes with high volume of GGBFS show better performance than silica fume-based mixes. This is because GGBFS-based mixes not only resist degradation more effectively (silica fume-based mixes have a denser microstructure and a less stable pore structure, which can lead to higher thermal stress and consequently, greater strength loss), but also significantly facilitate the formation of rehydration products.

5. Conclusions

This paper focused on evaluating the effect of different post-fire curing regimes on HSECC specimens with a possibility to broaden the understanding in this area. A comparison of the recovery is measured on five types of HSECC mixes with varying binder type and fibre content. This was assessed by conducting a series of tests including uniaxial compression, elastic modulus, SEM, XRD, TGA/DSC and MIP to explore

the effect of temperature on mechanical properties and microstructural characteristics of HSECC. Based on the observations, the following conclusions can be drawn:

- 28-day post-fire re-curing in air did not lead to any significant increase in compressive strength or elastic modulus. This was consistent for all the types of mixes irrespective of the fibre content or the matrix type. Microstructural analysis further showed minimal or no presence of rehydration phases in specimens subjected to air re-curing.
- Post-fire re-curing in water was found to significantly improve the residual compressive strength and elastic modulus for specimens exposed to temperatures above 400°C, with the recovery increasing as the re-curing duration was extended. However, for the specimens exposed to 200°C, water re-curing had a detrimental effect. The exact reason for this was not entirely clear, and further detailed studies would be needed to investigate the underlying mechanism and potential for improvement.
- Following water re-curing, mixes M1 and M4 exhibited high residual compressive strength, with more than 100 % strength retention at 600°C and approximately 62 % retention at 800°C. This confirms that mixes containing only GGBFS or blends of FA, dolomite, and GGBFS can lead to a substantial increase in residual strength after water re-curing. Mix M5, which used silica fume as the primary binder, also showed significant strength improvements after water re-curing. However, its overall recovery was less pronounced than the other mixes, likely due to the greater extent of decomposition caused by thermal exposure.
- Post-fire re-curing in water also led to a significant rise in the stiffness of the matrix. Significant recovery was observed for M1-M4 mixes in the residual elastic modulus with around 67–76 % retention at 800°C. Mix M5 showed the lowest improvement as expected with only 61 % retention at this temperature.
- Microstructural analysis further confirmed the formation of new phases as a result of rehydration. Formation of hydration products such as ettringite, portlandite and calcium silicate hydrates was observed especially for 400–800°C exposed specimens. These compounds were further confirmed through SEM micrographs, which revealed the widespread presence of ettringite and portlandite filling large pores. This pore filling contributed to a denser microstructure and a refined pore size distribution.

The findings from this study clearly demonstrate a strong potential of short duration water-re-curing to restore the strength of fire-damaged HSECC, with all tested blends demonstrating notable strength recovery. Additionally, the results highlight that the use of GGBFS blends in HSECC may be more beneficial for applications related to elevated temperature. Such blends not only retain higher residual strength, but also exhibit substantial recovery potential. Future investigations should delve into how post-fire re-curing impacts the performance of structural elements made from HSECC, thereby broadening the practical applicability of this material and re-curing procedure.

CRediT authorship contribution statement

S. Rawat: Writing – original draft, Conceptualization, Methodology, Investigation, Formal analysis, Visualization. **C. K. Lee:** Conceptualization, Supervision, Resources, Writing – review & editing. **D.J. Fanna:** Visualization, Writing – review & editing. **L. George:** Visualization, Writing – review & editing. **Y. X. Zhang:** Supervision, Resources, Writing – review & editing.

Declaration of Competing Interest

The authors declare that they have no known competing financial interests or personal relationships that could have appeared to influence the work reported in this paper.

Acknowledgment

Commonwealth's support for this research received through Australian Government RTP and UNSW Canberra's support through UIPA Scholarship are gratefully acknowledged. The authors would also like to acknowledge the Advanced Materials Characterisation Facility (AMCF), Western Sydney University for access to instrumentation and training.

Data Availability

Data will be made available on request.

References

[1] C.S. Poon, S. Azhar, M. Anson, Y.L. Wong, Strength and durability recovery of fire-damaged concrete after post-fire-curing, Cem. Concr. Res. 31 (9) (2001) 1307–1318, https://doi.org/10.1016/S0008-8846(01)00582-8.
[2] A.H. Akca, N. Özyurt, Effects of re-curing on microstructure of concrete after high temperature exposure, Constr. Build. Mater. 168 (2018) 431–441, https://doi.org/10.1016/j.conbuildmat.2018.02.122.
[3] M. Vyšvařil, P. Bayer, M. Chromá, P. Rovnaníková, Physico-mechanical and microstructural properties of rehydrated blended cement pastes, Constr. Build. Mater. 54 (2014) 413–420, https://doi.org/10.1016/j.conbuildmat.2013.12.021.
[4] H. Wang, H. Lyu, T. Liu, Y. Li, K.H. Tan, Effect of post-fire curing on compressive strength of ultra-high performance concrete and mortar, Constr. Build. Mater. 346 (2022) 128447, https://doi.org/10.1016/j.conbuildmat.2022.128447.
[5] Y. Li, H. Wang, C. Shi, D. Zou, A. Zhou, T. Liu, Effect of post-fire lime-saturated water and water–CO2 cyclic curing on strength recovery of thermally damaged high-performance concrete with different silica contents, Cem. Concr. Res. 164 (2023) 107050, https://doi.org/10.1016/j.cemconres.2022.107050.
[6] G.H. Nalon, J.C.L. Ribeiro, E.N.D. de Araújo, L.G. Pedroti, J.M.F. de Carvalho, R. F. Santos, D.S. de Oliveira, Effects of post-fire curing on the mechanical properties of cement composites containing carbon black nanoparticles and multi-walled carbon nanotubes, Constr. Build. Mater. 310 (2021) 125118, https://doi.org/10.1016/j.conbuildmat.2021.125118.
[7] H. Suh, S. Cho, S. Im, J. Moon, J. Park, J. Lim, E.Z. Nezhad, S. Seok, B.I. Bae, S. Bae, Characterization of thermal resistance and mechanical strength recovery of carbon nanotubes incorporated Portland cement composites subjected to heating and rehydration: Visualization of pore structural evolutions via synchrotron 3D X-ray nanoimaging, Cem. Concr. Compos. 146 (2024) 105361, https://doi.org/10.1016/j.cemconcomp.2023.105361.
[8] T. Liu, H. Wang, D. Zou, X. Long, M.J. Miah, Y. Li, Strength recovery of thermally damaged high-performance concrete subjected to post-fire carbonation curing, Cem. Concr. Compos. 143 (2023) 105273, https://doi.org/10.1016/j.cemconcomp.2023.105273.
[9] L. Li, L. Shi, Q. Wang, Y. Liu, J. Dong, H. Zhang, G. Zhang, A review on the recovery of fire-damaged concrete with post-fire-curing, Constr. Build. Mater. 237 (2020) 117564, https://doi.org/10.1016/j.conbuildmat.2019.117564.
[10] Z. Zhang, S. Liu, F. Yang, Y. Weng, S. Qian, Sustainable high strength, high ductility engineered cementitious composites (ECC) with substitution of cement by rice husk ash, J. Clean. Prod. 317 (2021) 128379, https://doi.org/10.1016/j.jclepro.2021.128379.
[11] K. Tosun-Felekoğlu, E. Gödek, M. Keskinateş, B. Felekoğlu, Utilization and selection of proper fly ash in cost effective green HTPP-ECC design, J. Clean. Prod. 149 (2017) 557–568, https://doi.org/10.1016/j.jclepro.2017.02.117.
[12] D. Zhang, B. Jaworska, H. Zhu, K. Dahlquist, V.C. Li, Engineered Cementitious Composites (ECC) with limestone calcined clay cement (LC3), Cem. Concr. Compos. 114 (2020) 103766, https://doi.org/10.1016/j.cemconcomp.2020.103766.
[13] Y. Deng, C. Yan, J. Zhang, L. Yin, S. Liu, Y. Yan, Preparation and mechanical characterization of engineered cementitious composites with high-volume fly ash and waste glass powder, J. Clean. Prod. 333 (2022) 130222, https://doi.org/10.1016/j.jclepro.2021.130222.
[14] M. Hou, D. Zhang, V.C. Li, Material processing, microstructure, and composite properties of low carbon Engineered Cementitious Composites (ECC), Cem. Concr. Compos. 134 (2022) 104790, https://doi.org/10.1016/j.cemconcomp.2022.104790.
[15] J. Yu, H.L. Wu, C.K. Leung, Feasibility of using ultrahigh-volume limestone-calcined clay blend to develop sustainable medium-strength Engineered Cementitious Composites (ECC), J. Clean. Prod. 262 (2020) 121343, https://doi.org/10.1016/j.jclepro.2020.121343.
[16] S. Rawat, Y.X. Zhang, C.K. Lee, Multi-response optimization of hybrid fibre engineered cementitious composite using Grey-Taguchi method and utility concept, Constr. Build. Mater. 319 (2022) 126040, https://doi.org/10.1016/j.conbuildmat.2021.126040.
[17] S. Rawat, C.K. Lee, Y.X. Zhang, Green engineered cementitious composites with enhanced tensile and flexural properties at elevated temperatures, Clean. Mater. 12 (2024) 100240, https://doi.org/10.1016/j.clema.2024.100240.

[18] S. Rawat, Y.X. Zhang, D.J. Fanna, C.K. Lee, Development of sustainable engineered cementitious composite with enhanced compressive performance at elevated temperatures using high volume GGBFS, J. Clean. Prod. 451 (2024) 142011, https://doi.org/10.1016/j.jclepro.2024.142011.
[19] S. Rawat, Y.X. Zhang, C.K. Lee, Spalling Resistance of Hybrid Polyethylene and Steel Fiber-Reinforced High-Strength Engineered Cementitious Composite (2023), in: W. Duan, L. Zhang, S.P. Shah (Eds.), Nanotechnology in Construction for Circular Economy. NICOM 2022. Lecture Notes in Civil Engineering, 356, Springer, Singapore, 2022, https://doi.org/10.1007/978-981-99-3330-3_33.
[20] X. Ming, M. Cao, X. Lv, H. Yin, L. Li, Z. Liu, Effects of high temperature and post-fire-curing on compressive strength and microstructure of calcium carbonate whisker-fly ash-cement system, Constr. Build. Mater. 244 (2020) 118333, https://doi.org/10.1016/j.conbuildmat.2020.118333.
[21] H. Suh, H. Jee, J. Kim, R. Kitagaki, S. Ohki, S. Woo, K. Jeong, S. Bae, Influences of rehydration conditions on the mechanical and atomic structural recovery characteristics of Portland cement paste exposed to elevated temperatures, Constr. Build. Mater. 235 (2020) 117453, https://doi.org/10.1016/j.conbuildmat.2019.117453.
[22] H. Suh, S. Im, J. Kim, S. Bae, Instant mechanical recovery of heat-damaged nanosilica-incorporated cement composites under various rehydrations procedures, Mater. Struct. 55 (1) (2022) 5, https://doi.org/10.1617/s11527-021-01847-y.
[23] S. Rawat, C.K. Lee, Y.X. Zhang, Performance of fibre-reinforced cementitious composites at elevated temperatures: A review, Constr. Build. Mater. 292 (2021) 123382, https://doi.org/10.1016/j.conbuildmat.2021.123382.
[24] X. Wang, Y. Peng, J. Wang, Q. Zeng, Pore structure damages in cement-based materials by mercury intrusion: A non-destructive assessment by X-ray computed tomography, Materials 12 (14) (2019) 2220, https://doi.org/10.3390/ma12142220.
[25] G.F. Peng, Z.S. Huang, Change in microstructure of hardened cement paste subjected to elevated temperatures, Constr. Build. Mater. 22 (4) (2008) 593–599, https://doi.org/10.1016/j.conbuildmat.2006.11.002.
[26] C. Alonso, L. Fernandez, Dehydration and rehydration processes of cement paste exposed to high temperature environments, J. Mater. Sci. 39 (9) (2004) 3015–3024, https://doi.org/10.1023/B:JMSC.0000025827.65956.18.
[27] Q. Ma, R. Guo, Z. Zhao, Z. Lin, K. He, Mechanical properties of concrete at high temperature—A review, Constr. Build. Mater. 93 (2015) 371–383, https://doi.org/10.1016/j.conbuildmat.2015.05.131.
[28] Q. Zhang, G. Ye, Dehydration kinetics of Portland cement paste at high temperature, J. Therm. Anal. Calorim. 110 (1) (2012) 153–158, https://doi.org/10.1007/s10973-012-2303-9.
[29] S.K. Handoo, S. Agarwal, S.K. Agarwal, Physicochemical, mineralogical, and morphological characteristics of concrete exposed to elevated temperatures, Cem. Concr. Res. 32 (7) (2002) 1009–1018, https://doi.org/10.1016/S0008-8846(01)00736-0.
[30] D.N. Crook, M.J. Murray, Regain of strength after firing of concrete, Mag. Concr. Res. 22 (72) (1970) 149–154, https://doi.org/10.1680/macr.1970.22.72.149.
[31] M. Henry, K. Hashimoto, I.S. Darma, T. Sugiyama, Cracking and chemical composition of cement paste subjected to heating and water re-curing, J. Adv. Concr. Technol. 14 (4) (2016) 134–143, https://doi.org/10.3151/jact.14.134.
[32] G. Wang, C. Zhang, B. Zhang, Q. Li, Z. Shui, Study on the high-temperature behavior and rehydration characteristics of hardened cement paste, Fire Mater. 39 (8) (2015) 741–750, https://doi.org/10.1002/fam.2269.